Available online at www.sciencedirect.com
SCIENCE DIRECT®
Journal of Theoretical Biology 230 (2004) 499–519
Journal of Theoretical Biology
www.elsevier.com/locate/jtbi

Apparent discontinuities in the phase-resetting response of cardiac pacemakers

T. Krogh-Madsen[a], L. Glass[a,*], E.J. Doedel[b], M.R. Guevara[a]

[a] Department of Physiology, Centre for Nonlinear Dynamics, McGill University, Montreal, 3655 Drummond Street, Que., Canada H3G 1Y6
[b] Department of Computer Science, Concordia University, Montreal, Que., Canada H3G 1M8

Received 15 December 2003; received in revised form 19 March 2004; accepted 22 March 2004

Available online 23 July 2004

Abstract

Injection of a brief stimulus pulse resets the spontaneous periodic activity of a sinoatrial node cell: a stimulus delivered early in the cycle generally delays the time of occurrence of the next action potential, while the same stimulus delivered later causes an advance. We investigate resetting in two models, one with a slow upstroke velocity and the other with a fast upstroke velocity, representing central and peripheral nodal cells, respectively. We first formulate each of these models as a classic Hodgkin–Huxley type of model and then as a model representing a population of single channels. In the Hodgkin–Huxley-type model of the slow-upstroke cell the transition from delay to advance is steep but continuous. In the corresponding single-channel model, due to the channel noise then present, repeated resetting runs at a fixed stimulus timing within the transitional range of coupling intervals lead to responses that span a range of advances and delays. In contrast, in the fast-upstroke model the transition from advance to delay is very abrupt in both classes of model, as it is in experiments on some cardiac preparations (''all-or-none'' depolarization). We reduce the fast-upstroke model from the original seven-dimensional system to a three-dimensional system. The abrupt transition occurs in this reduced model when a stimulus transports the state point to one side or the other of the stable manifold of the trajectory corresponding to the eigendirection associated with the smaller of two positive eigenvalues. This stable manifold is close to the slow manifold, and so canard trajectories are seen. Our results demonstrate that the resetting response is fundamentally continuous, but extremely delicate, and thus suggest one way in which one can account for experimental discontinuities in the resetting response of a nonlinear oscillator.

Keywords: Resetting; Canard; Ionic model; Sinoatrial node; Single channels

''It is my belief that the life sciences in particular have much to gain from, and perhaps something to contribute to, mathematical developments in the general area of topology''. Winfree (1980).

1. Introduction

One of the central premises of Art Winfree's masterpiece, *The Geometry of Biological Time* (Winfree, 1980, 2000), is that the language of topologists can be used to ''extract from models or from observations what seems to be the essence of their behavior, independent of quantitative variations''. This attitude, which was revolutionary in 1980, is perhaps even more so today. The exponential growth of computer power, combined with refined experimental methods, makes it possible to develop increasingly accurate mathematical models of the behaviors of biological systems at all size scales ranging from the subcellular to the ecological. But computations with a mathematical model that can simulate perfectly the behavior of some biological system under a given experimental condition might offer no more insight than simply carrying out the experiment.

The topological approach offers almost magical insights into the analysis of the resetting of biological oscillators. In a resetting experiment, a stimulus is

*Corresponding author. Tel.: +1-514-398-4338; fax: +1-514-398-7452.
E-mail address: glass@cnd.mcgill.ca (L. Glass).

0022-5193/$ - see front matter © 2004 Elsevier Ltd. All rights reserved.
doi:10.1016/j.jtbi.2004.03.027

delivered to an oscillator and its effects on the oscillator are characterized as the magnitude and timing of the stimulus are systematically varied. Resetting experiments have been undertaken in all fields of biology in which oscillations are found (Winfree, 1980, 2000). Winfree showed that under the assumption that the oscillation can be described by a differential equation, the types of resetting response that are found can be characterized topologically. Consequently, it is possible to make predictions about the response of biological oscillations to perturbation even without knowing anything about the details of the biology. Indeed, the qualitative, topological features of the resetting observed in some very simple models are amazingly similar to those which are observed in experiments. In particular, this topological approach of Winfree's stimulated experimentalists to successfully search for two important phenomena in cardiac electrophysiology: annihilation (the permanent cessation of spontaneous activity in a cardiac pacemaker induced by injection of a well-timed stimulus pulse (Jalife and Antzelevitch, 1979)) and the induction of spiral-wave reentry in a distributed medium by a similarly well-timed stimulus (Chen et al., 1988).

In an effort to test the predictions of the topological approach, and also to compute the effects of periodic stimulation on cardiac oscillators, our group has characterized the resetting of electrical activity in spontaneously beating aggregates of embryonic chick ventricular cells (Glass et al., 1984; Guevara et al., 1986). One set of data, shown in Fig. 1. (reproduced from Guevara et al., 1986) poses a problem for the topological approach. Fig. 1 shows the resetting effect of a single current pulse delivered to a spontaneously beating aggregate at three different times in the cycle. When the stimulus is delivered on several trials at 141 ms after the upstroke of the immediately preceding action potential (Fig. 1A, top panel), then the timing of the next action potential is always delayed, i.e. the action potential following the stimulus occurs later than one would expect from the unperturbed oscillation. In contrast, when the same stimulus is delivered at 143 ms after the action potential (Fig. 1A, bottom panel), the timing of the next action potential is always advanced, since the action potential occurs promptly after delivery of the stimulus. However, when the stimulus is delivered many times at 142 ms after an action potential (Fig. 1A, middle panel; Fig. 1B), either one or the other of these two responses is observed (i.e. no intermediate responses are seen). Further, at the end of the trace, which occurs several cycle lengths following delivery of the stimulus, there is still a distinct maintained difference between the two sets of responses (Fig. 1A, middle panel).

Our goal in this article is to make clear why the observations in Fig. 1 pose a sharp problem for the topological approach, to suggest an explanation of the observed behavior, and to consider the implications of these observations. In Section 2, we give the necessary definitions and notation for presenting data from resetting experiments. In Section 3, we develop two different classes of mathematical models for simulating cardiac oscillations (a classic Hodgkin–Huxley-type model and a model composed of a population of single channels). The results of simulations using these models are presented in Section 4 and discussed in Section 5.

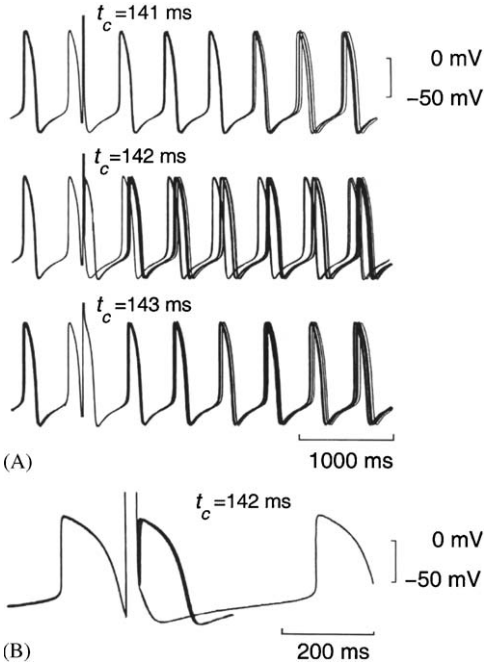

Fig. 1. Resetting experiment in a spontaneously beating aggregate of embryonic chick ventricular heart cells (diameter = 149 μm). The transmembrane potential is plotted as a function of time. (A) A depolarizing stimulus of amplitude 27 nA and duration 20 ms is delivered multiple times at a coupling interval t_c (time from the immediately preceding action potential upstroke to the start of the stimulus) indicated above each set of traces. (B) Zoom-in on the 11 trials conducted at a coupling interval of 142 ms: three of these produced prolongation of cycle length; the other 8 produced abbreviation. Superimposed traces are aligned on the upstroke of the action potential occurring immediately before stimulus injection. Notice that the individual traces in (A) are so close that they are indistinguishable for the first few cycles. The large off-scale voltage deflections during delivery of the stimulus pulse are artifact due to the fact that the same intracellular microelectrode is used to deliver the stimulus current as to record the transmembrane potential, with imperfect bridge-balance. Adapted from Guevara et al. (1986) with permission.

2. Mathematical background for analysis of resetting data

Since biological oscillations often have quite stationary periods and amplitudes (e.g. the coefficient of variation (standard deviation/mean) of the interbeat interval of an isolated sinoatrial node pacemaker cell is

on the order of 2.0% (Wilders and Jongsma, 1993)), it is usual to associate the oscillation with a stable limit cycle in the phase space of some appropriate nonlinear model of the oscillation (Winfree, 1980, 2000). Recall that a *stable limit cycle* is a periodic solution of a differential equation that is attracting in the limit of $t \to \infty$ for all points in a neighborhood of the limit cycle. Say that the period of the oscillation is T_0. We will designate an arbitrary point on the limit cycle to be the fiducial point, with the phase (ϕ) at that point being zero. Starting a trajectory from that point at $t = 0$, the *phase* of any point on that trajectory (which will follow the limit cycle) at a subsequent time $t > 0$ is defined to be $\phi = t/T_0 \pmod 1$. The phase here is thus constrained to lie between 0 and 1; to convert it to radians multiply it by 2π.

The set of all initial conditions that attract to the limit cycle in the limit $t \to \infty$ is called the *basin of attraction* of the limit cycle. Let a point $x(t)$ be on the limit cycle at time t and another point $y(t)$ be in the basin of attraction of that limit cycle. Denote the distance between x and y by $d[x, y]$. Let the phase of x at $t = 0$ be ϕ. Then, if in the limit $t \to \infty$, $d[x(t), y(t)] \to 0$, the *latent* or *asymptotic* or *eventual* phase of $y(t)$ is also ϕ. We say that $y(t)$ is on the same *W-isochron* as $x(t)$. The development of the concept of W-isochrons and the recognition of their significance is due to Winfree (Winfree, 1970, 1980, 2000). Many mathematical results concerning W-isochrons were established by Guckenheimer (Guckenheimer, 1975), who considered dynamical systems in n-dimensional Euclidean space.

We now consider the effect of a stimulus delivered to a biological oscillator. In general, delivery of a stimulus will perturb the state of the oscillator, so that its period transiently changes, but with the initial period becoming reestablished asymptotically in time. This process corresponds to the stimulus perturbing the state point of the system away from the limit cycle, followed by the asymptotic return of the state point back to the limit cycle. However, the trajectory will in general asymptotically approach a point on the limit cycle that has a different phase (the *new phase*) from that of the initial starting point on the limit cycle (the *old phase*). There will thus be a *resetting* of the phase of the oscillation (*phase-resetting*). Assume that a perturbation delivered to an oscillation at an (old) phase ϕ shifts the oscillation to a new phase $g(\phi)$. The function $g(\phi)$ is called the *phase transition curve*. The following *Continuity Theorem* summarizes important aspects of the effects of a stimulus on limit cycle oscillations in ordinary differential equations (Guckenheimer, 1975) and partial differential equations (Gedeon and Glass, 1998). If a stimulus of a given amplitude delivered at any old phase of a limit-cycle oscillation leaves the state point within the basin of attraction of that asymptotically stable limit cycle, then the phase transition curve will be continuous for that stimulus amplitude.

The phase transition curve $g(\phi)$ is a circle map $g : S^1 \to S^1$. Circle maps can be continuous or discontinuous. A continuous circle map $f(\phi)$ can be characterized by its (*topological*) *degree* or *winding number*. The degree of $f(\phi)$ is the number of times that $f(\phi)$ wraps around the unit circle as ϕ goes around the circle once. For very weak perturbations, $g(\phi) \approx \phi$ by continuity, and the degree of the phase transition curve is 1. In many instances, as Winfree discusses (Winfree, 1970, 1980, 2000), the degree of the phase transition curve is 0 when the stimulation is sufficiently strong. If the degree of the resetting curve is 1 for weak stimuli and 0 for strong stimuli, there must be an intermediate stimulus strength (or range of strengths) that will result in the state point of the system being perturbed to a location outside of the basin of attractor of the limit cycle—though whether the trajectory eventually reattains the limit cycle depends on whether the stimulus perturbs the state point into the basin of attraction of yet another stable attractor. Similarly, if the phase transition curve is truly discontinuous there must be a stimulus phase or range of stimulus phases that will result in the state point being perturbed outside of the basin of attraction of the limit cycle (Gedeon and Glass, 1998).

In phase space, a curve can be constructed that is the locus of state points at the end of a stimulus for any old phase. This curve is the *shifted cycle*. In the case where the shifted cycle intersects all the W-isochrons of the limit cycle, there is type 1 resetting. On the other hand, if the stimulus is of sufficiently strong amplitude to move the shifted cycle to a location where it no longer intersects all W-isochrons, type 0 resetting will occur (see further discussion in Guevara and Jongsma, 1990).

These abstract notions can be directly translated into a protocol that allows the phase transition curve to be experimentally determined. A typical resetting simulation for a cardiac pacemaker is shown in Fig. 2. In this case a depolarizing stimulus is given at a coupling interval t_c, which is measured from the crossing of the

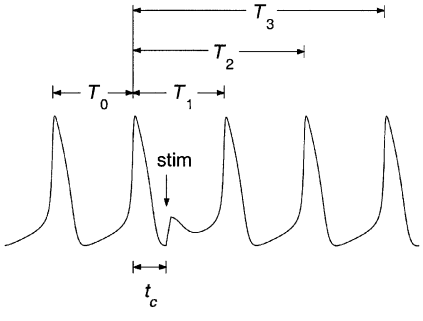

Fig. 2. Notation for resetting protocol in a schematic sinoatrial node cell. A depolarizing stimulus is given at a coupling interval t_c after the crossing of 0 mV on the upstroke of the second action potential. The (old) phase of the cycle at which the stimulus is delivered is t_c/T_0. This stimulus causes a delay, with the first perturbed cycle length, T_1, being larger than the unperturbed period, T_0.

0 mV level on the immediately preceding action potential upstroke to the onset of the stimulus pulse. This positive-going crossing of 0 mV corresponds to the fiducial point on the limit cycle having an old phase (ϕ) of zero. In the case of Fig. 2, the stimulus causes the interbeat interval to be prolonged (i.e. $T_1 > T_0$). The intervals T_1, T_2, and T_3 in the figure are defined as the times between the initial crossing of 0 mV on the upstroke of the action potential and subsequent positive-going crossings of 0 mV (the *event marker*). We will refer to the interval T_1 as the *perturbed cycle length*. With the definitions in the figure, the old phase ϕ and the i-th *transient new phases* ϕ_i, $i \geqslant 1$ are given by

$$\phi = \frac{t_c}{T_0} \pmod 1,$$
$$\phi_i = \phi + \frac{iT_0 - T_i}{T_0} \pmod 1. \quad (1)$$

The new phase is defined to be ϕ_i in the limit $i \to \infty$. Also in the limit $i \to \infty$, $T_{i+1} - T_i \to T_0$ as the perturbed trajectory asymptotically approaches the limit cycle.

With this background we can now pose the dilemma presented by the data in Fig. 1. The experimentally determined phase transition curve is discontinuous, since the asymptotic phase has two very different values for a stimulus given at coupling intervals of 141 and 143 ms (Fig. 1A, top and bottom panels). Indeed, there is overlap in the curve (i.e. $g(\phi)$ is not single-valued), since a stimulus given at a fixed coupling interval of 142 ms results in one of two different types of response, with no intermediate responses being seen (Fig. 1A, middle panel; Fig. 1B). Moreover, all stimuli given to this preparation are followed by the eventual reestablishment of the spontaneous oscillation, showing that each stimulus left the state point within the basin of attraction of the limit cycle.

One possible resolution of these findings is that the phase transition curve is really continuous, but because the isochrons are very closely packed, the old phase, and so the coupling interval, would have to be changed with an extraordinarily fine gradation to observe the continuity. However, the electrical activity of the aggregate is noisy: e.g. the interbeat interval of the cycle immediately preceding stimulus injection (first cycle in Fig. 1A) fluctuates from trial to trial, as does the trajectory during the perturbed cycle for the entire time preceding delivery of the stimulus (the superimposed traces of multiple trials in Fig. 1 are thicker than the trace from a single trial). There is thus effectively some degree of scanning of the old phase occurring even when t_c is kept fixed at 142 ms (± 1 μs).

One problem here is thus that the fundamental hypothesis underlying Winfree's theory is not satisfied: spontaneous activity in the aggregate is not well-described by a system of noise-free differential equations. Rather, spontaneous activity corresponds to a noisy limit cycle, with the noise being generated internally by the stochastic opening and closing of a finite number of ionic channels (each of finite conductance) lying within the membrane. This fact led us to propose many years ago that the unitary nature of the ion channels underlying the electrical activity of the aggregate should be taken into account in constructing a realistic model to be used for resetting simulations (Guevara et al., 1986). In the next section, we develop Hodgkin–Huxley-type models as well as single-channel population models to explore this idea.

3. Methods

3.1. Hodgkin–Huxley-type models

Although we would have preferred to analyse an ionic model for the electrical activity in an aggregate of embryonic chick ventricular heart cells (Fig. 1), such a model is not presently available. Consequently, we investigate resetting phenomena in a model of a different cardiac pacemaker—the sinoatrial node. We have developed two models of a single sinoatrial node cell that we study below. In the following, we shall refer to these two Hodgkin–Huxley-type models as the "noise-free models". Both of these models (see Appendix A for details) are modifications of the Irisawa–Noma sinoatrial node model (Irisawa and Noma, 1982), which has five currents: the fast inward sodium current (I_{Na}), the slow inward current (I_s) carried mainly by Ca^{2+} ions, the delayed rectifier potassium current (I_K), the pacemaker current (I_h), and the time-independent leak current (I_l). One of the major differences between the central and more peripheral areas of the node is that the maximal upstroke velocity of the action potential is much higher in the more peripheral areas. Thus, one of our models (the "slow-upstroke model") has a very small I_{Na} and a very slow upstroke velocity (5 V s^{-1}), while the other model (the "fast-upstroke model") has a much bigger I_{Na} and so a much faster upstroke velocity (71 V s^{-1}). As we shall see below, these changes result in significant differences in the resetting properties of the two models.

3.2. Single-channel population models

The behavior in Fig. 1B shows that one of two results is seen in repeated resetting trials carried out at a fixed coupling interval. We had previously hypothesized that this apparently random response is due to the fact that the electrical activity in the aggregate is not deterministic, but stochastic, stemming from the action potential being generated by a population of single channels, each of which opens and closes in a stochastic fashion (Guevara et al., 1986). We thus wish to re-formulate

our noise-free ionic model (above) into a model with a finite number of channels (the parent noise-free ionic model can then be thought of as describing a cell that in the limit possesses an infinite number of channels, each of vanishingly small conductance, but with the total conductance remaining finite). A model of a single sinoatrial node cell formulated as a population of single channels (which we shall term a "single-channel model") has previously been implemented using a very detailed ionic model (Wilders and Jongsma, 1993) as well as a simplified version of the Irisawa–Noma model (Guevara and Lewis, 1995). This latter minimal model simulated a population of I_K and I_s channels. Since our models include I_{Na} and I_h in addition to I_K and I_s, we now add back to the minimal single-channel model a population of I_{Na} and I_h channels to restore these two currents present in the original Irisawa–Noma model. Appendix B provides further details about the computational methods used to implement the single-channel models.

3.3. Continuation methods

Associated with the discontinuous response in the experiment of Fig. 1B is an abrupt transition from delay to advance in the noise-free model. To investigate the nature of this abrupt transition we reduced the seven-dimensional fast upstroke model to a three-dimensional model, where we can compute and visualize the stable and unstable manifolds of the fixed point, which are one- and two-dimensional, respectively.

The stable manifold of the fixed point can be calculated by accurate integration in backward time. The unstable manifold of the fixed point can, in principle, be accurately computed by integrating in forward time a discrete set of points that lie in a small circle in the unstable eigenspace in the neighborhood of the fixed point. However, due to the large differences in the magnitudes of the two positive eigenvalues, the orbits are sensitively dependent on the initial conditions. This would result typically in large portions of the unstable manifold not being swept out. This deficiency is remedied using AUTO to apply continuation to the entire orbit as an object in function space (Doedel et al., 1997).

4. Results

4.1. Spontaneous activity in slow- and fast-upstroke models

We modify the original Irisawa–Noma model (Irisawa and Noma, 1982) to produce a slow-upstroke model and a fast-upstroke model (see Methods and Appendix A for further description). In the slow-upstroke model, the maximal upstroke velocity is $5\,Vs^{-1}$, the overshoot potential is 18 mV, the maximal diastolic potential is −66 mV, the action potential duration (to 100% repolarization) is 137 ms, and the interbeat interval is 338.2 ms. These values are close to those reported previously for the unmodified Irisawa–Noma model (Guevara and Jongsma, 1990; Irisawa and Noma, 1982). Fig. 3 (left column) shows spontaneous activity in the corresponding single-channel model. There is cycle-to-cycle variability in the various traces.

In comparison with the slow-upstroke model, the fast-upstroke model has a much larger maximal upstroke velocity ($71\,Vs^{-1}$), a larger overshoot potential (31 mV), a more hyperpolarized maximum diastolic potential (−78 mV), a shorter action potential duration (86 ms), and a shorter interbeat interval (282.6 ms). These changes are consistent with those found experimentally when comparing in situ activity in central and peripheral areas of the sinoatrial node (Bleeker et al., 1980; Kodama and Boyett, 1985; Kreitner, 1985; Opthof et al., 1987), and when comparing activity in smaller single sinoatrial node cells (which presumably come from the center of the node) with larger ones (which presumably come from the periphery) (Honjo et al., 1996; Lei et al., 2001; Zhang et al., 2000). The increased I_{Na} in the fast-upstroke model increases the maximal upstroke velocity, while the increased I_K shortens the action potential duration (despite the increased I_s) and hyperpolarizes the maximum diastolic potential, thereby also increasing the maximal upstroke velocity further due to greater voltage-dependent removal of inactiva-

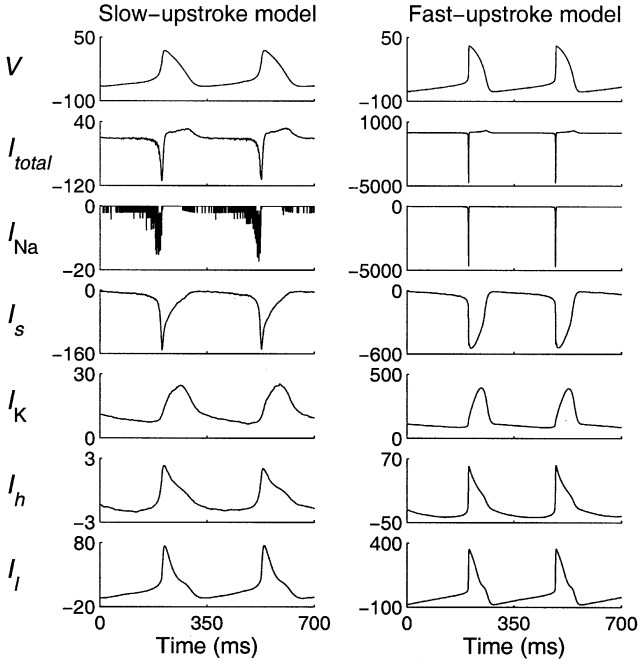

Fig. 3. Spontaneous activity in the single-channel slow-upstroke model (left) and the single-channel fast-upstroke model (right). Voltage is in mV and current in pA. Note change in scale for the currents (especially I_{total} and I_{Na}).

tion of I_{Na}. The increased I_h and I_s contribute to a steeper pacemaker potential, while the increased I_{Na} hyperpolarizes the threshold potential; both of these effects thus contribute to the shortening of the interbeat interval. The I_s waveform is very different in the two models due to the rectification of I_s.

Fig. 3 (right column) shows the activity in the corresponding single-channel model of a fast-upstroke cell. The fact that the number of channels is larger in the fast-upstroke model than in the slow-upstroke model accounts for the greater regularity of beating of the former (the coefficient of variation of inter beat interval is 1.5% in the former, 4.0% in the latter). Part of this increase in regularity is due to the greater size (65 vs. 20 pF) and hence increased number of channels in the fast-upstroke cell. By itself, this difference would be expected to cause an increase in regularity by a factor of $\sqrt{65/20}$ to 2.2% (Clay and DeHaan, 1979; Wilders, 1993). However, the increased channel density of several currents in the fast-upstroke model (see Appendix A) causes an additional increase in regularity, decreasing the coefficient of variation further to 1.5%.

The embryonic chick ventricular aggregate used in Fig. 1 is very similar to a peripheral sinoatrial node cell in terms of the particular mix of currents present in the cell membrane. Therefore, the voltage waveforms are alike in the two types of preparations. Specifically, the chick aggregates also have a fast upstroke and a relatively hyperpolarized maximum diastolic potential.

For both the slow- and the fast-upstroke models there is only one crossing of the voltage-axis in the steady-state total current–voltage plot, and thus there is only one fixed point in the seven-dimensional phase space of the system. In both cases numerical integration starting out from an initial condition close to the fixed point results in the eventual resumption of spontaneous activity, suggesting that the fixed point is unstable. Computation of eigenvalues using AUTO (Doedel et al., 1997) confirms that this is indeed the case. The eigenvalues show that the fixed point is a saddle in both models: two eigenvalues are real and positive, while the remaining five are real and negative.

4.2. Resetting in the slow-upstroke model

Fig. 4 shows the T_i (left column) and the first (middle column) and second (right column) transient phase transition curves obtained from the slow-upstroke model at three values of the stimulus amplitude for a pulse duration of 20 ms. The third transient phase (not shown) was essentially equal to the second, implying that the state point returns to the vicinity of the limit cycle relatively quickly. These phase transition curves are very similar to those found previously in the original Irisawa–Noma model (Guevara and Jongsma, 1990) and show characteristic features such as: (a) a change

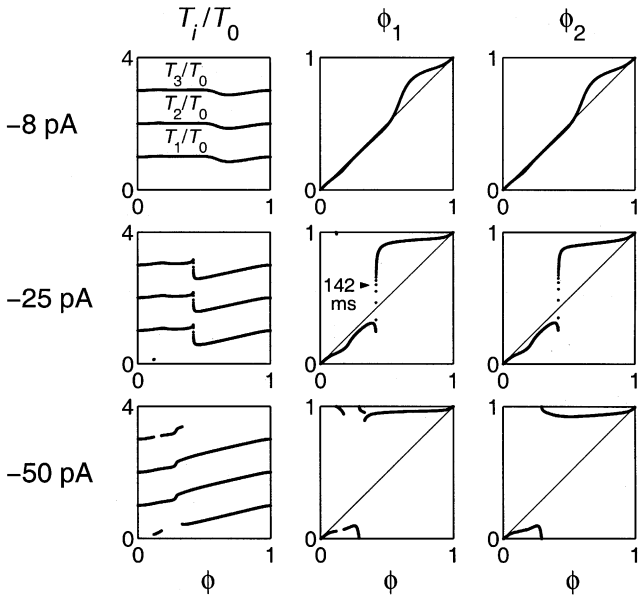

Fig. 4. Resetting curves from the slow-upstroke model. Left column: normalized first, second, and third perturbed cycle lengths (T_1/T_0, T_2/T_0, T_3/T_0); middle column: first transient phase (ϕ_1); right column: second transient phase (ϕ_2). Upper row shows type 1 resetting (stimulus amplitude = −8 pA) as does the middle row (stimulus amplitude = −25 pA). The lower row shows type 0 resetting (stimulus amplitude = −50 pA). Negative current indicates a depolarizing stimulus; stimulus duration = 20 ms. Arrowhead indicates point corresponding to the value of t_c used in the next two figures. Coupling interval was incremented in steps of 1 ms in the top row and 0.1 ms in the middle and bottom rows.

from type 1 (Fig. 4, top and middle rows) to type 0 (Fig. 4, bottom row) resetting as the stimulus amplitude is increased; (b) a decrease in the old phase at which the transition from prolongation to abbreviation of the perturbed cycle length (T_1) occurs with increasing stimulus amplitude; and (c) a steeper transition from prolongation to abbreviation during type 1 resetting as the stimulus amplitude is increased. These features are also observed in experiments on the sinoatrial node (see e.g. Jalife et al., 1980) and on aggregates (Glass et al., 1984; Guevara et al., 1986; Vanmeerwijk et al., 1984). Although the phase transition curve does get steeper as the stimulus amplitude is increased, we were always able to resolve the curves using increments in t_c down to 0.1 ms. Because of transient effects associated with the definition of the event marker, T_1 and ϕ_1 show discontinuities: see for example the bottom left and middle panels in Fig. 4 (for a discussion see Kawato (1981) and Kawato and Suzuki, 1978). However, the new phase is determined by the asymptotic value of ϕ_i (Eq. (1)) and the discontinuities associated with transient effects will not appear here. Indeed, no discontinuity is detectable in the plot of ϕ_2 vs. ϕ (Fig. 4, right column) on the scale of that figure.

We next investigate resetting in the single-channel version of the slow-upstroke model. Fig. 5 shows

responses to a stimulus of amplitude −25 pA and duration 20 ms at three different coupling intervals. This is the same stimulus amplitude and duration used in the middle row of Fig. 4. For $t_c = 132$ ms, prolongation of cycle length is observed in 10 of 10 trials (Fig. 5A), while for $t_c = 152$ ms, abbreviation of cycle length is observed in 10 of 10 trials (Fig. 5C). There is an intermediate range of t_c over which, at a fixed value of t_c, some trials result in prolongation while others result in abbreviation, with a large spread in the response: e.g. at $t_c = 142$ ms (arrowhead in Fig. 4) there is abbreviation in 6 of 10 trials (Fig. 5B). Increase in t_c over this intermediate range results in a greater fraction of trials resulting in abbreviation.

A zoom-in on the voltage at the end of the stimulus delivered ten times at $t_c = 142$ ms in Fig. 5B shows an interesting effect due to the single-channel fluctuations (Fig. 6). The dashed trace shows a response that resulted in an abbreviation of cycle length (Fig. 6, top trace).

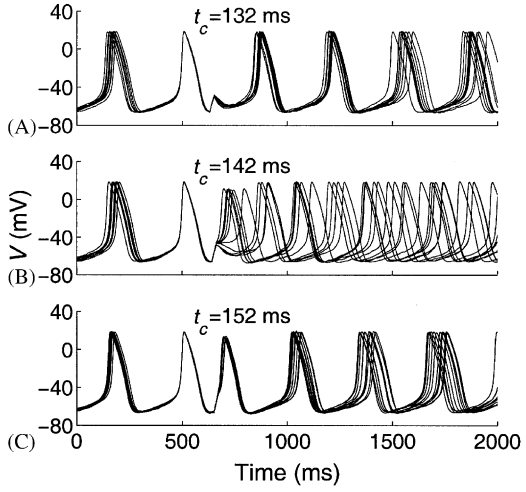

Fig. 5. Resetting in the single-channel slow-upstroke model. Same stimulus amplitude (−25 pA) as used in noise-free model in the middle row of Fig. 4. Stimulus duration = 20 ms. For each value of t_c, 10 superimposed runs are shown, aligned on the upstroke of the action potential immediately preceding stimulus injection.

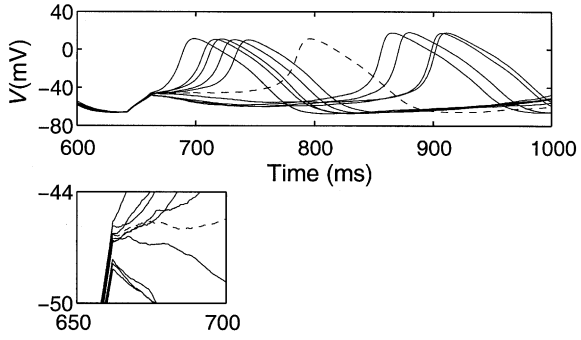

Fig. 6. Zoom of multiple trials in resetting simulations for t_c=142 ms (Fig. 5B) showing "fuzzy threshold".

However, this response paradoxically started out with a more depolarized potential at the end of the stimulus pulse than two of the other responses that ended up firing sooner (Fig. 6, bottom trace). The concept of a sharp threshold voltage thus does not hold here. This type of "fuzzy threshold" must be due to an effect involving one or more of the variables apart from the voltage: e.g., if I_s at the end of the stimulus in the dashed trace is more inactivated than on average, the membrane may not fire even though one would think that the voltage is sufficiently depolarized for it to do so. Alternatively, the delay in firing might be caused by fluctuations in the state of the population of channels after the end of the stimulus. There could be again an increased inactivation of I_s, increased activation of an outward current such as I_K, and/or one or more of several other effects.

4.3. Resetting in the fast-upstroke model

In the fast-upstroke model, as was the case in the slow-upstroke model, the transition from prolongation to abbreviation of cycle length becomes steeper with increasing stimulus amplitude. However, in the fast-upstroke model, the transition eventually becomes so steep that it cannot be resolved using an increment in t_c as small as 0.1 μs (Fig. 7, middle row). We refer to this behavior in what follows as the "abrupt transition". For an even higher stimulus amplitude, type 0 resetting occurs (Fig. 7, bottom row). This pattern of changes in the features of the response for increasing stimulus amplitude has been observed in other ionic

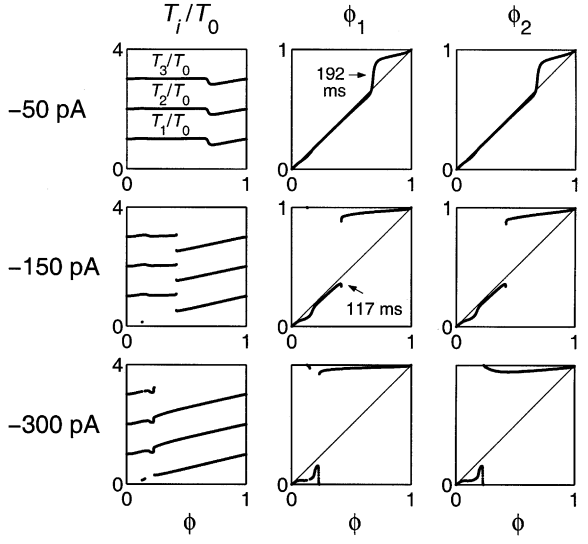

Fig. 7. Resetting in the fast-upstroke model. Notice abrupt transition in phase transition curves with stimulus amplitude = −150 pA (middle row). Stimulus duration = 20 ms. Arrows indicate points used in resetting in the corresponding single-channel model in the next two figures. Coupling interval was incremented in steps of 0.1 ms, 0.1 μs around the abrupt transition in the middle row.

models in which the upstroke of the action potential is caused by I_{Na} (Clay et al., 1984, 1990; Guevara and Shrier, 1987).

In the corresponding single-channel fast-upstroke model, one observes the responses shown in Fig. 8 at the lowest amplitude used in Fig. 7 (−50 pA, top row). (It can also be appreciated from this figure that the regularity of beating is greater here than in the slow-upstroke single-channel model (Fig. 5)). When a value of t_c is chosen that lies in the steep part of the phase transition curve (Fig. 7, top row) a mixed response occurs: abbreviation of cycle length occurs in 8 of 10 trials at $t_c = 192$ ms, with prolongation in the remaining two trials (Fig. 8B). For $t_c = 182$ ms (Fig. 8A) there is only prolongation of cycle length, while for $t_c = 202$ ms (Fig. 8C) there is only abbreviation. This type of behavior is also seen in embryonic chick ventricular aggregates when the stimulus amplitude is of intermediate size (see e.g. Fig. 2–18 of Guevara, 1984).

At a higher stimulus amplitude (−150 pA), where the phase transition curve has an abrupt transition in the noise-free model (Fig. 7, middle row), an abrupt transition also occurs in the single-channel model. At $t_c = 117$ ms, 5 of 10 trials show abbreviation, while the other 5 of 10 trials show prolongation (Fig. 9B). Indeed, in 1000 trials at this coupling interval we did not observe a single intermediate response: the histogram of the latency from the end of the stimulus pulse to 0 mV on the upstroke of the next action potential is bimodal (Fig. 10). Decreasing t_c by 1 ms causes prolongation in 10 of 10 trials (Fig. 9A), while increasing t_c by 1 ms results in abbreviation in 10 of 10 trials (Fig. 9C). This modelling result is analogous to the experimental response in Fig. 1.

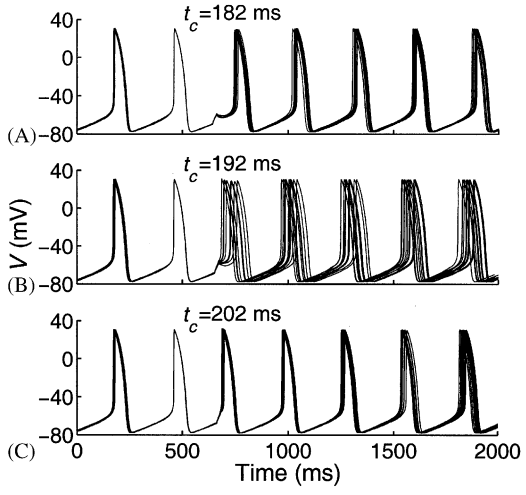

Fig. 8. Resetting in single-channel fast-upstroke model. Same stimulus parameters as in Fig. 7, top row: stimulus amplitude = −50 pA, stimulus duration = 20 ms. Ten trials shown for each value of coupling interval (t_c).

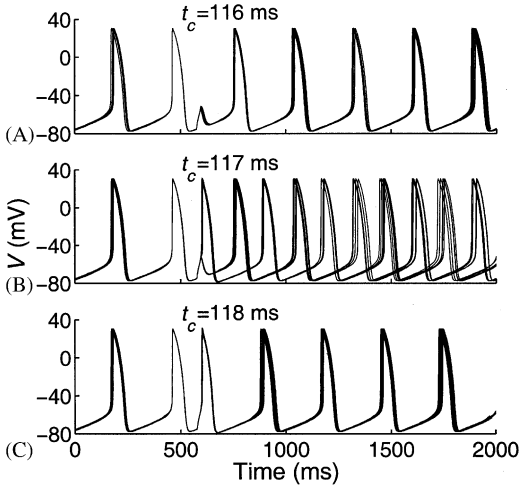

Fig. 9. Resetting in single-channel fast-upstroke model. Same stimulus parameters as in Fig. 7, middle row: stimulus amplitude = −150 pA, stimulus duration = 20 ms. Notice abrupt transition at $t_c = 117$ ms. Ten trials shown for each value of coupling interval (t_c).

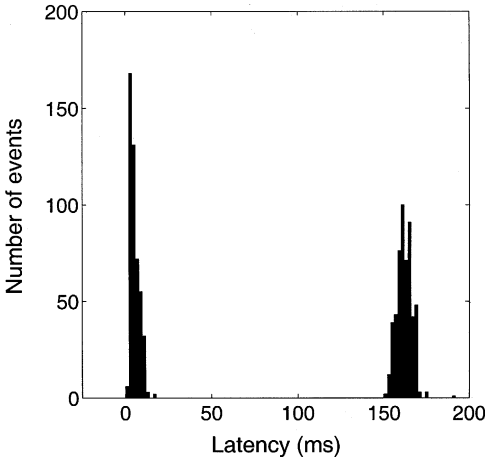

Fig. 10. Histogram of 1000 trials in single-channel fast-upstroke model. Histogram gives the number of action potentials occurring at a given latency from end of stimulus pulse. Stimulus amplitude −150 pA, pulse duration = 20 ms, $t_c = 117$ ms.

Notice that the noise-induced irregularity in the intrinsic interbeat interval in the fast-upstroke model is sufficiently small to allow the two types of response induced in Fig. 9B to persist in time (the two groups of traces are easily distinguishable by eye several cycles following delivery of the stimulus). The fuzzy threshold effect seen for the slow-upstroke model (Fig. 6) is not evident here, although we expect that it exists. This is presumably due to two factors: the decreased noise in the fast-upstroke model and the increased speed and size of I_{Na} (responsible for the upstroke phase in the fast-upstroke model) in comparison to I_s (responsible for the upstroke phase in the slow-upstroke model).

Thus, the major difference in the resetting response of the fast-upstroke noise-free model and the corresponding single-channel model is that in the former the phase transition curve is single-valued, with an abrupt transition at one precise value of the old phase. In the latter case, over a very narrow critical range of the old phase centered on the abrupt transition, there are two narrow ranges of new-phase values, separated by an effectively forbidden gap. This clustering effect of the noise has also been observed in the Hodgkin–Huxley model of the quiescent squid axon with added voltage noise (Clay, 1977).

4.4. The abrupt transition in a reduced fast-upstroke model

An abrupt transition in the resetting response is seen in both experiment (Fig. 1B) and in the fast-upstroke model (Fig. 7, middle row; Figs. 9B and 10). Since it is difficult to visualize trajectories in the phase space of the fast-upstroke model because it is seven-dimensional, we study them in two simplified models. We first investigate the abrupt transition more finely in a reduced three-dimensional ionic model, and then provide a theoretical interpretation by investigating a linear three-dimensional model.

The reduction of the seven-dimensional fast-upstroke model to a three-dimensional model is obtained by making several approximations. First, we remove I_h since it contributes very little current to the total current. Second, because the time-constants τ_m and τ_d are quite small, we set the activation variables of I_{Na} (m) and I_s (d) equal to their asymptotic or steady-state values ($m_\infty = \alpha_m/(\alpha_m + \beta_m)$ and $d_\infty = \alpha_d/(\alpha_d + \beta_d)$ respectively). The time constants for activation of I_K (τ_p) and inactivation of I_s (τ_f) are of the same order of magnitude, and p and f essentially vary out-of-phase with respect to each other, so that one can express either one in terms of the other: $p = 0.36 - 0.27f$. (The idea of making this approximation comes from work in the Hodgkin–Huxley model of the squid giant axon, where $n = 0.85 - h$, with n being the activation variable for I_K and h being the inactivation variable for I_{Na} (FitzHugh, 1961).) There are then only three state variables left in the model: V (transmembrane voltage), h (inactivation variable for I_{Na}), and f (inactivation variable for I_s). To maintain the same upstroke velocity as in the seven-dimensional model (71 V s^{-1}), the maximal conductance of I_{Na} was reduced to 73% of its original value. To maintain the intrinsic cycle length the maximal conductance of I_K was reduced to 65% of its original value. This caused an increase in the action potential duration of less than 10%.

As in the full seven-dimensional model, there is again a range of stimulus amplitudes over which the transition from prolongation to abbreviation of cycle length is very abrupt with a change in t_c as small as 0.1 μs. We investigate this transitional range more finely in the reduced three-dimensional model by probing with increments in t_c of <0.1 μs. Fig. 11A shows several resetting runs: the top set of traces show increasing prolongation of cycle length as t_c is changed to several values lying between 85 and 85.336376727283 ms (red trace), while the bottom set of traces show increasing abbreviation of cycle length as t_c is further changed between 85.336376727284 ms (blue trace) and 86 ms. There is thus still an abrupt transition between prolongation (upper panel, red trace) and abbreviation (bottom panel, blue trace) of cycle length even with a change in t_c as minuscule as 10^{-12} ms. Very similar results are found in the seven-dimensional model.

The simulations in Fig. 11A show an extreme sensitivity of the dynamics as t_c is changed very finely. The main effect of a small increase in t_c in Fig. 11A is to depolarize the membrane further at the end of the stimulus pulse by a small amount. Thus, an increment in the voltage at the end of the stimulus pulse can be used to mimic the effect of an increment in t_c. For example, artificially increasing the voltage in this manner by 3×10^{-12} mV at the end of a pulse delivered at $t_c = 85.336376727283$ ms causes the prolongation seen at that value of t_c (red trace in Fig. 11A) to change into abbreviation. To quantify this behavior we carried out simulations in which we explored initial conditions very close to locations reached at the end of the stimuli that lead to the red and blue curves in Fig. 11A. We vary V in increments as fine as 10^{-14} mV around the value $V^* = -49.35457869225426$ mV, which is the voltage at the end of the stimulus when maximal prolongation is observed (red trace in Fig. 11A). In Fig. 11B, we plot the time t_1 from the end of the stimulus pulse to the start of the next action potential (defined here as the crossing of -30 mV) as a function of $\ln|V - V^*|$. The upper curve of points gives t_1 when a prolongation occurs (because $V \leqslant V^*$), while the lower set of points gives t_1 when an abbreviation occurs (because $V > V^*$). Both curves approximate straight lines when V is close to V^* (i.e. for $\ln|V - V^*|$ small). A similar result is found in the original seven-dimensional model.

The main reason we develop the reduced three-dimensional model is that it is then possible to compute and visualize important geometric features in the phase space. Fig. 11C shows trajectories in the three-dimensional phase space of the system. The black closed curve is the unperturbed limit cycle. The trajectories corresponding to the maximal prolongation and abbreviation seen in Fig. 11A (red and blue traces with $t_c = 85.336376727283$ ms and $t_c = 85.336376727284$ ms, respectively) are also shown. In both cases the stimulus takes the state point from a neighborhood of the location labelled "A" on the limit cycle and delivers it to the neighborhood of location "B" (the purple color of

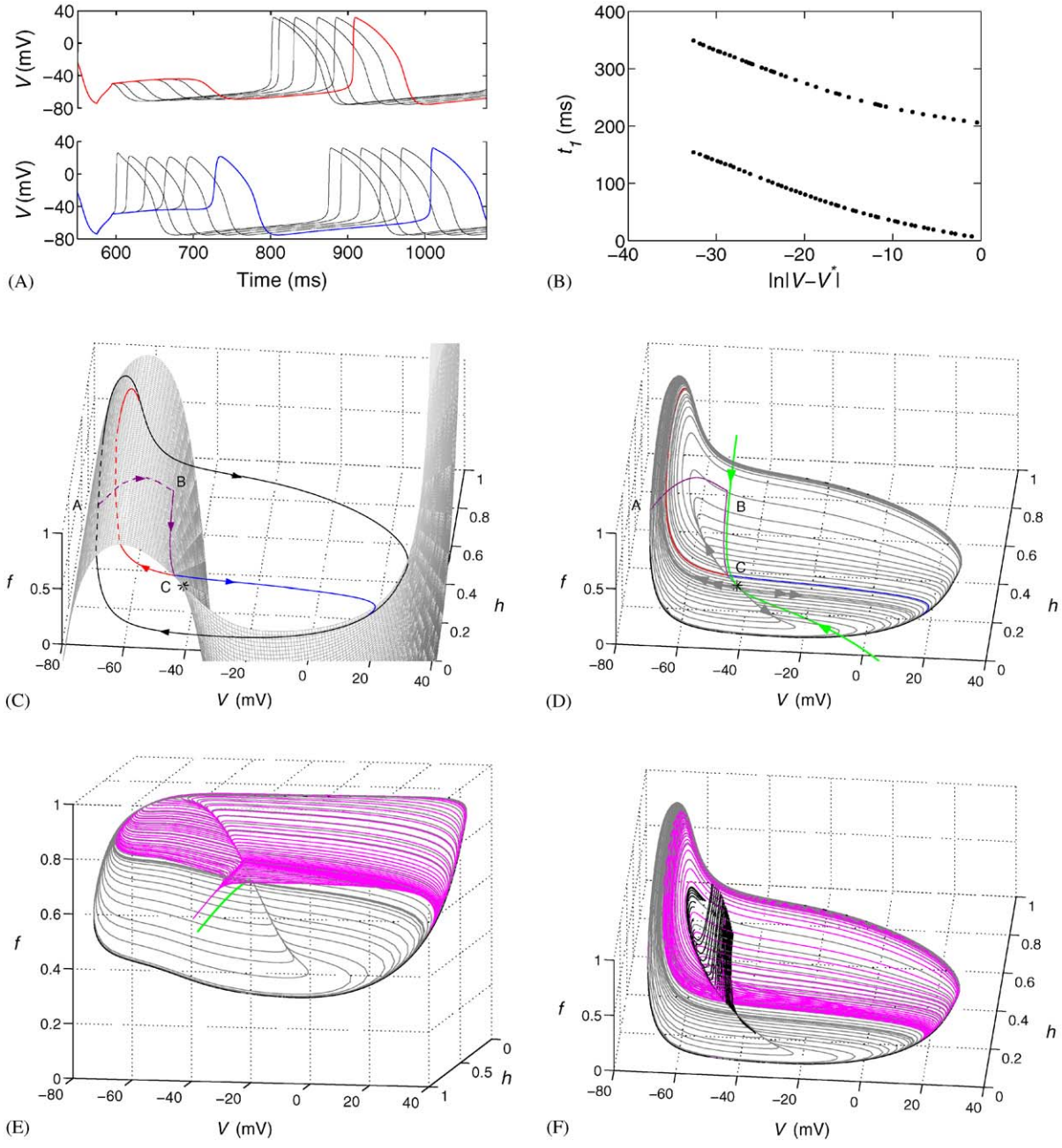

Fig. 11. Resetting in reduced three-dimensional fast-upstroke model. (A) Voltage traces with t_c spanning a range from 85.0 ms to 85.336376727283 ms (red trace) in upper panel, and 85.336376727284 ms (blue trace) to 86.0 ms in lower panel. Stimulus amplitude = −150 pA, pulse duration = 20 ms. (B) Time taken for trajectories to cross $V = -30$ mV (t_1, "escape time") as a function of displacement of V from the fiducial value V^*. The upper set of points are for prolongation, bottom for abbreviation. (C) Phase-space trajectories corresponding to the red and blue responses shown in (A). The shaded two-dimensional surface is the slow manifold (given by $dV/dt = 0$). (D) The green curve gives the stable manifold of the fixed point, while the gray trajectories lie within the unstable manifold. (E) Trajectories (magenta) obtained by continuation from a set of very close initial conditions near location "B" in (C). Gray trajectories lie within the unstable manifold. (F) Stable manifold of the weak unstable manifold (black trajectories). See text for further description. For larger, rotatable color figures, please visit www.cnd.mcgill.ca/bios/glass/glass_j2004-2006.htm.

the trajectory indicates that the blue and red trajectories lie very close to one another, being superimposed on the scale of this diagram). Point "B" is very close to the slow manifold of the system (the shaded gray two-dimensional surface defined by $dV/dt = 0$). For $t_c = 85.336376727283$ ms, immediately following the end of the stimulus, the state point moves from location "B", staying close to the slow manifold for some time (purple trajectory) before deviating to the left (at location "C"), producing a prolongation of cycle length (red trajectory). In contrast, for $t_c = 85.336376727284$ ms, while the state point also stays

close to the slow manifold for about the same length of time (purple trajectory), it then takes off rapidly to the right (blue trajectory) from location "C", resulting in a graded action potential (an action potential with smaller overshoot potential and slower maximal upstroke velocity) and an abbreviation of cycle length. As t_c is increased beyond 85.336376727284 ms, the abbreviation of cycle length gets more marked as the trajectory stays close to the slow manifold for shorter periods of time, taking off to the right and leaving the purple trajectory earlier. As t_c is decreased below 85.336376727283 ms the amount of prolongation decreases as the trajectory takes off to the left and leaves the vicinity of the slow manifold earlier. These trajectories which run along close to the slow manifold and then diverge from its vicinity are canards (a canard is an exceptional trajectory, characterized by partly lying along the unstable segment of a slow manifold, see e.g. Arima et al., 1997; Diener, 1984; Guckenheimer et al., 2000).

During the time that the trajectory lingers close to the slow manifold in Fig. 11C (from location "B" to location "C"), $\mathrm{d}V/\mathrm{d}t$ is very small, and thus the voltage trace is almost flat following the end of the stimulus pulse for both abbreviation and prolongation (Fig. 11A). Although a small value of $\mathrm{d}V/\mathrm{d}t$ could also have been produced if the state point were knocked into the vicinity of the fixed point (located at the coordinates $(V,h,f) = (-40.703, 0.007, 0.567)$, indicated by $*$ in Fig. 11C) by the stimulus, this is not occurring here, since location "B" is relatively far removed from the fixed point.

The eigenvalues of the fixed point are all real, two are positive (195, 5) and one is negative (-77), so that the fixed point is a saddle of index 2. The stable manifold is therefore a one-dimensional curve, which is shown in Fig. 11D (green curve). When the abrupt transition of Figs. 11A,C occurs, the trajectories are much closer to the slow manifold than to the stable manifold of the fixed point. The unstable manifold of the fixed point is a two-dimensional surface, and the gray curves in Fig. 11D are trajectories, computed by continuation, that lie within this unstable manifold. The eigendirection associated with the eigenvalue 195 is called u_s, the eigendirection associated with the eigenvalue 5 is called u_w. The two trajectories which are collinear with u_s near the fixed point are called the *strong unstable manifold* (double arrows in Fig. 11D). In a linear system, as we shall see later, u_w plays an important role as the eigendirection from which trajectories diverge. However, in the nonlinear model all trajectories, except the pair that defines the strong unstable manifold, are tangent to u_w at the fixed point, and so the *weak unstable manifold* is not uniquely defined. For most of our purposes a visual definition of the weak unstable manifold as the curve from which trajectories diverge will suffice (single arrows in Fig. 11D), but for one of our computations we employ a strict definition (see last paragraph of this section). For $t_c = 85.336376727283$ ms and 85.336376727284 ms, the trajectories come very close to the unstable manifold of the fixed point before deviating in directions parallel to the strong unstable manifold (red and blue trajectories in Fig. 11D).

With an increment in t_c of 10^{-12} ms or in $|V - V^*|$ of 10^{-14} mV, we are at the limits of the precision of our numerical integration routine. However, we can probe the abrupt transition more finely using continuation techniques. We start at a point in phase space very close to where the blue trajectory ends up at the end of the stimulus pulse (near location "B" in Figs. 11C,D) and generate trajectories that start along a short line of initial conditions passing through that point, parallel to the V-axis. The maximal and minimal values of V along this line are chosen such that the maximal value is slightly larger than the voltage resulting from the blue trajectory (V_b), while the minimal value is slightly smaller than the voltage resulting from the red trajectory (V_r).

Fig. 11E shows the results. As in Fig. 11D, the gray trajectories lie within the unstable manifold. The magenta curves are trajectories that start off from the short line of initial conditions close to "B". Notice that this figure has been rotated relative to Figs. 11C,D to improve visualization (the original projection is shown again in Fig. 11F). As seen in Fig. 11D, the trajectories initially run more-or-less parallel to the stable manifold of the fixed point (green curve) and then zip off to the left or to the right. As the initial V-value decreases towards V_b, or similarly, as the initial V-value increases towards V_r, the point where trajectories diverge ("the take-off point") moves further towards the unstable manifold. A fan of trajectories is thus generated consisting of trajectories which fall almost into a plane approximately parallel to the (V, h)-plane. Decreasing V from V_b or increasing V from V_r, one eventually reaches a point where the take-off point leaves the neighborhood of the slow manifold and makes its way along the weak unstable manifold (seen as the curve from which trajectories diverge) in the direction of increasing f. Further decreasing V from V_b or increasing V from V_r results in the trajectories following the weak unstable manifold for a longer time before abruptly leaving it. Eventually the take-off point enters a region at the very top of the figure where trajectories coming off the weak unstable manifold are no longer sharply diverging. Thus, using the continuation technique, we have been able to resolve the apparent discontinuity (Fig. 11A) and demonstrate the fundamental underlying continuity of the resetting response.

Since trajectories diverge from the weak unstable manifold, we conjecture that this divergence occurs because of the existence of a stable manifold of the weak unstable manifold. (Notice that this is not a stable manifold in the usual sense since a trajectory starting out on it will go to the limit cycle as $t \to \infty$ rather than staying on the weak unstable manifold. However,

trajectories on this stable manifold will get arbitrarily close to the weak unstable manifold. This use of the terminology is consistent with previous usage (e.g. Wiggins, 1988, pp. 355–356)). The abrupt transition then occurs when a stimulus brings the state point to one side or the other of the stable manifold of the weak unstable manifold. To compute this stable manifold, the weak unstable manifold must be unique and well-defined. We employ the following definition: *the trajectories which have the maximal integration time when integrating from a small sphere of initial conditions around the fixed point to a constant distance away from the fixed point lie within the weak unstable manifold.* There will be two local maxima in the integration time identifying two trajectories which are both tangent to the weak eigendirection, but going in opposite directions. This definition thus uses the fact that state points move slowly in the weak eigendirection. This definition has the advantage that we can use existing continuation methods in AUTO to compute the weak unstable manifold and its stable manifold. The black curves in Fig. 11F are trajectories lying within the stable manifold of the weak unstable manifold. While trajectories that approach the unstable manifold, e.g. the blue and the red trajectories (Figs. 11A,D) do indeed lie in the vicinity of the stable manifold of the weak unstable manifold, the computations are not sufficiently accurate to determine whether the stable manifold of the weak unstable manifold separates diverging trajectories.

4.5. A linear three-dimensional model

Although the three-dimensional model given above is much simpler than the original seven-dimensional model, it is still complex. Much of the dynamics seen in Figs. 11C–F occurs in the neighborhood of a three-dimensional saddle of index two. Consequently, we have explored the dynamics of a linear three-dimensional saddle of index two.

The equations

$$\frac{dx}{dt} = \frac{1}{\varepsilon}(x - y),$$
$$\frac{dy}{dt} = x,$$
$$\frac{dz}{dt} = -\frac{1}{\mu} z,$$

where $0 < \varepsilon < \mu \ll 1$, result in a saddle of index two being present at the origin. The eigenvalues are

$$\lambda_1 = \frac{1}{2\varepsilon}(1 + \sqrt{1 - 4\varepsilon}),$$
$$\lambda_2 = \frac{1}{2\varepsilon}(1 - \sqrt{1 - 4\varepsilon}),$$
$$\lambda_3 = -\frac{1}{\mu}.$$

For $0 < \varepsilon \ll 1$, we have $\lambda_1 \gg \lambda_2 > 0$, while for $\mu > 0$, we have $\lambda_3 < 0$.

We associate x with V in our simulations above, and when x crosses over the line $x = x_c = 5$, we associate this with the crossing of -30 mV in the simulations of Fig. 11B when a shortening of cycle length is seen. We will examine stimuli that take the state point from the limit cycle to the point $(x, y, z) = (y_0 + \delta, y_0, z_0)$, where $0 < y_0 < x_c - \delta$ and $z_0 > 0$. Since z is decoupled from x and y, the solution for x of the linear three-dimensional differential equation does not depend on z

$$x(t) = c_1 e^{\lambda_1 t} + c_2 e^{\lambda_2 t}.$$

From the initial condition we compute

$$c_1 = \frac{1}{\lambda_1 - \lambda_2}(\delta\lambda_1 - y_0\lambda_2),$$
$$c_2 = \frac{1}{\lambda_1 - \lambda_2}(-\delta\lambda_2 - y_0\lambda_1).$$

Further, for initial conditions that lie along the eigendirection corresponding to the smaller positive eigenvalue, $c_1 = 0$ and the x-dynamics will be given by $x(t) = c_2 e^{\lambda_2 t}$. This occurs for initial conditions $(x, y, z) = (y_0 + \delta_0, y_0, z_0)$, where

$$\delta_0 = \frac{\lambda_2 y_0}{\lambda_1}.$$

We can now compute the dynamics for an initial condition $(x, y, z) = (y_0 + \delta_0 + \eta, y_0, z_0)$ and compute the time, t_1 until an action potential, i.e. until $x(t) = x_c$. For $\lambda_1 \gg \lambda_2$, we find

$$t_1 = \frac{1}{\lambda_1}\left(-\ln \eta - \ln\left(\frac{\lambda_1}{\lambda_1 - \lambda_2}\right) + \ln(x_c - c_2)\right). \tag{2}$$

For an initial condition that has (x, y)-coordinates near the eigendirection associated with λ_2 (the weak unstable eigendirection, u_w), the trajectory is attracted towards the (x, y)-plane quickly and then moves along the weak unstable eigendirection for some time before diverging in the eigendirection associated with λ_1 (the strong unstable eigendirection, u_s). Such trajectories are shown in Figs. 12A–C for $\varepsilon = 0.02$, $\mu = 0.07$, $y_0 = z_0 = 0.5$, and η varying from $\pm 10^{-16}$ to $\pm 10^{-3}$ (the values of ε and μ were chosen to give eigenvalues (49, $\sim$1, -15), which have relative magnitudes similar to those in the three-dimensional ionic model (195, 5, -77)). The three straight lines in Fig. 12A passing through the origin are the eigendirections. The dashed line (Fig. 12C) lies in the x-nullsurface defined by $dx/dt = 0$ (this surface is the two-dimensional analog in a three-dimensional system of the one-dimensional nullcline in a two-dimensional system). The x-nullsurface corresponds to the unstable segment of the slow manifold in the nonlinear ionic model (Fig. 11C). In Fig. 12C, for $\eta < 0$ trajectories start off with (x, y)-coordinates to the left of the weak unstable eigendirection and eventually diverge from this eigendirection towards the left (i.e. in the direction of

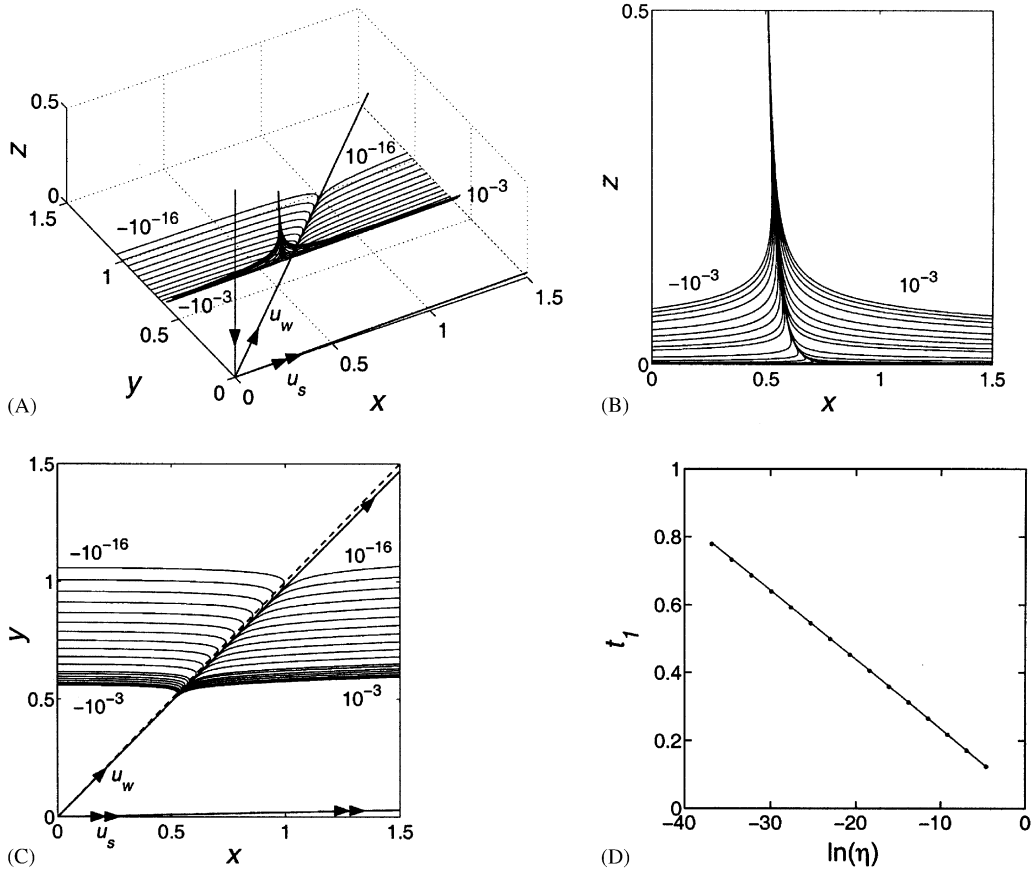

Fig. 12. Dynamics in three-dimensional linear model. (A) Phase space trajectories in simple three-dimensional model. Numbers give values of displacement from the δ_0 line (η). Straight lines with arrows represent the eigendirections. (B) Projection onto the (x,z)-plane. (C) Projection onto the (x,y)-plane. Dashed line indicates the projection of the x-nullsurface (defined by $dx/dt = 0$). (D) Time until crossing of $x = 5$ ("escape time", t_1) as a function of ln(η), calculated from Eq. (2) (solid line) and from simulations (dots).

decreasing x). In contrast, for $\eta > 0$, initial state points lie to the right of the weak unstable eigendirection and trajectories eventually turn right, away from this eigendirection. In this linear model, the stable manifold of the weak unstable eigendirection is simply the plane defined by $y = x/\lambda_2$, since the weak unstable eigenvector is given by $[x\ y\ z]^T = [1\ \ 1/\lambda_2\ \ 0]^T$. Therefore, initial conditions with (x, y)-coordinates on either side of the weak unstable eigendirection are in fact separated by the stable manifold of the weak unstable eigendirection, in a manner analogous to that seen in the three-dimensional ionic model (Fig. 11F).

The symbols in Fig. 12D show the time until an action potential in the linear model as a function of ln(η), for $\eta > 0$. These results coincide with the straight line giving the analytical result (Eq. (2)). We can now compare our analysis of the slope of the t_1 vs. ln(η) plot for the three-dimensional linear saddle with the slope of the t_1 vs. $\ln|V - V^*|$ plot for the ionic models. The linear approximation in the latter nonlinear cases is expected to be best when the trajectory lies closest to the fixed point. Thus we take the slope of the lower plot in Fig. 11B at the smallest values of that plot. (Escape times were computed for trajectories from numerical integration only and not from continuation. Therefore, escape times shown in Fig. 11B are from the "fan"-structure of Fig. 11E and not from trajectories that visibly track the weak unstable manifold. However, at least in the three-dimensional linear model, the escape time has the same linear dependence on ln(η) for trajectories in the fan as well as for those that track the weak unstable manifold for longer durations.) The negative reciprocal of the slope in Fig. 11B is 167, which compares well with the largest positive eigenvalue (195). For the full seven-dimensional ionic model the largest eigenvalue is 99 and the negative reciprocal of the slope of the t_1 vs. $\ln|V - V^*|$ plot is 102. These results provide justification for our view that the existence of a saddle point of index two accounts for much of the dynamics in the nonlinear ionic models.

5. Discussion

One of most compelling results of the topological approach of Winfree is the Continuity Theorem, which

states that the phase transition curve must be continuous, except for exceptionally timed stimuli that take the state point of the system outside of the basin of attraction of the limit cycle. However, when the response changes very rapidly with small changes in the coupling interval, careful probing over a narrow range of old phase is required in order to investigate the theoretically predicted continuity. Such experiments have rarely been carried out. When carried out in the chick ventricular cell aggregate, there is no sign of continuity, and, as explained earlier, the experimental result at $t_c = 142$ ms in Fig. 1 contradicts the Continuity Theorem. Here, using continuation methods, we have shown that the corresponding abrupt transition from prolongation to abbreviation (Fig. 11A) in the reduced ionic model is only an apparent discontinuity in that the response is really continuous (Fig. 11E).

5.1. Dynamics in phase space: QTP-separatrix and canards

In the linear three-dimensional model, diverging trajectories appear as trajectories which start on either side of the stable manifold of the weak unstable eigendirection (Figs. 12A,C). Since the stable manifold of the weak unstable eigendirection is very close to the x-nullsurface, state points moving along this stable manifold also travel in the vicinity of the x-nullsurface, producing canards. Similar behavior has been described in a piecewise-linear version of the two-dimensional FitzHugh–Nagumo model (Arima et al., 1997). The quantification of the rate of divergence in our simple model was found to correspond well with that observed in the three- and seven-dimensional nonlinear ionic models.

In the reduced three-dimensional ionic model, following the end of a well-timed stimulus pulse, trajectories initially move along very close to the slow manifold, producing canards (Fig. 11C). With even finer adjustment of t_c, the trajectories then move along the weak unstable manifold for some time until departing one way or the other (Fig. 11E). Our conjecture is that the abrupt transition occurs when the state point is perturbed into the vicinity of the stable manifold of the weak unstable manifold. At present, we have not been able to compute this stable manifold to an accuracy sufficient to prove this conjecture (Fig. 11F). Instead, a schematic illustration of the separation of trajectories is shown in Fig. 13. Trajectories come down in a fan parallel to the stable manifold of the fixed point, and are separated by the stable manifold of the weak unstable manifold (shaded surface).

Similar behavior with the trajectories hugging the unstable segment of the slow manifold has previously been described in the excitable (i.e. no limit cycle present) version of the two-variable FitzHugh–Nagumo

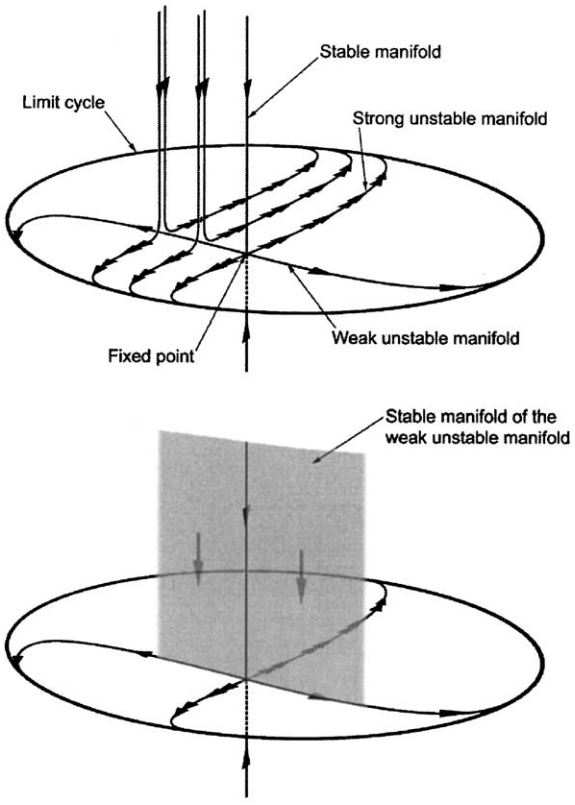

Fig. 13. Schematic representation of abrupt transition. Trajectories are separated by the stable manifold of the weak unstable manifold (shaded surface).

equations (FitzHugh, 1961). FitzHugh termed this apparently all-or-none response the quasi-threshold phenomenon (QTP) to contrast it to a true threshold phenomenon where the stable manifold of a saddle point acts as a separatrix, and the path (not uniquely defined) that separates the two classes of responses the QTP-separatrix (FitzHugh, 1955, 1961). Thus, the stable manifold of the weak unstable manifold in the three-dimensional system, plays the same role here as the QTP-separatrix in the two-dimensional example studied by FitzHugh. Three circumstances in which there can be discontinuities in the phase transition curve are when: (1) three fixed points are present, one of which is a saddle (Clay et al., 1984; Glass and Winfree, 1984); (2) the fixed point is a spiral point (Glass and Winfree, 1984); (3) there is a "black hole" (Glass and Winfree, 1984).

As was the case for the fast-upstroke model, the seven-dimensional slow-upstroke model can be reduced to a three-dimensional one (by setting $q = h = m = 0$ and $d = d_\infty$). The eigenvalues of the fixed point in this reduced model are 49, 8, and -3 (vs. 195, 5, and -77 for the reduced fast-upstroke model). Since the ratio of the two positive eigenvalues is not as big as in the fast-upstroke model, the nodal structure of the unstable manifold, with one strong and one weak unstable

manifold from which trajectories diverge (Figs. 11D, 12A,C and 13), is not as extreme. In addition, the stable eigendirection is not as strongly attracting and trajectories therefore do not approach the surface of the unstable manifold as easily. Hence, intermediate responses are more easily seen in the slow-upstroke model (Fig. 5, middle panel). It is also possible in the slow-upstroke model that a stimulus might deliver the state point sufficiently close to the stable manifold of the weak unstable manifold so as to produce an apparent discontinuity. However, changing stimulus amplitude in steps of 5 pA and coupling interval in steps of 0.01 ms, we have observed no jumps larger than 0.1 in the new phase in the slow-upstroke model.

While we have not investigated the phase space portrait in the full seven-dimensional fast-upstroke model, the close similarity of the voltage traces in the full model to those in the three-dimensional model (Fig. 11A) suggests that a very similar mechanism is operating in the seven-dimensional model. One noticeable difference between the resetting results in the two models is that in the seven-dimensional model, the abrupt transition occurs later on in the cycle (at $t_c \simeq 117$ ms in Fig. 7, middle panel and Fig. 9B vs. $t_c \simeq 85$ ms in Fig. 11A). The maximum diastolic potential is more hyperpolarized in the seven-dimensional model, so that after a longer t_c the membrane potential at the end of the stimulus is very similar to that at the end of the stimulus in the three-dimensional model. This suggests that the geometric structures causing the abrupt transition in the three-dimensional model are similarly placed in terms of V in the phase spaces of both models.

5.2. Ionic mechanisms underlying the abrupt transition

Our simulations with the full fast-upstroke model show that as stimulus amplitude is increased the transition from prolongation to abbreviation of cycle length becomes more abrupt to the point where it appears discontinuous (Figs. 7, 9, 10). A similar result occurs in experiment (see e.g. Glass et al., 1984; Guevara et al., 1986; Jalife and Moe, 1976). The abrupt transition from prolongation to abbreviation shown in Figs. 1 and 9 is reminiscent of classic all-or-none depolarization (Cole et al., 1970). The pulse with $t_c = 116$ ms (Fig. 9A) finds the membrane in a certain state and causes a certain amount of depolarization. When the pulse turns off, I_K and I_l repolarize the membrane. The same stimulus pulse delivered 2 ms later (Fig. 9C) finds the membrane in a different state: e.g. V is slightly more depolarized due to spontaneous diastolic depolarization, the activation variable of I_{Na} (m) is slightly larger due to voltage-dependent activation, the inactivation variable of I_{Na} (h) is slightly larger due to the time-dependent removal of inactivation (the oppositely directed voltage-dependent increase in inactivation is not sufficient to counterbalance this effect), and the activation variable for I_K (p) is smaller. The membrane resistance is also greater, since the currents I_K and I_l are turning off during diastolic depolarization, which contributes to the larger change in V produced by the stimulus. This increase in membrane resistance contributes to the membrane being more depolarized at the end of the stimulus pulse. During the pulse, I_{Na} is larger because of increased activation and decreased inactivation. At the time that the pulse is turned off, V lies at the foot of the m_∞ curve and the Hodgkin cycle results, leading to an almost immediate upstroke.

This abrupt transition has previously been seen in resetting studies using ionic models of Purkinje fibre (Guevara and Shrier, 1987) and the atrial aggregate (Clay et al., 1990), and in one partial model of the ventricular aggregate (Clay et al., 1984). In all of these cases, as well as in ours, there is a fight between the inward current I_{Na} and a net repolarizing current of comparable magnitude. The very rapid kinetics of I_{Na} makes the response very sensitive. For example, in the full noise-free fast-upstroke model at $t_c = 117.158751189269$ ms, where prolongation is seen, artificially depolarizing the membrane by a further 10^{-15} mV at the end of the stimulus pulse is sufficient to convert prolongation into abbreviation. At this point in the cycle, opening of a single Na^+-channel for 0.1 ms will depolarize the membrane by about 0.003 mV, while opening or closing of one of the other channel types for the same amount of time will change the membrane voltage by 10^{-6}–10^{-4} mV. Therefore, the opening or closing of a single channel would more than suffice to change prolongation to abbreviation or vice versa.

This sharp voltage dependence is reminiscent of the situation in the Hodgkin–Huxley equations, where an increase in the take-off potential of 0.2 mV suffices to convert a subthreshold response into a full-sized action potential and increments of 10^{-12} mV must be used to demonstrate the underlying continuity of the intervening graded responses (Clay, 1977). In the Hodgkin–Huxley equations, a difference in stimulus amplitude of 0.01 μA/cm^2 results in all-or-none behavior and a change in stimulus amplitude as small as 10^{-14} μA/cm^2 is needed to show the intermediate responses (FitzHugh and Antosiewicz, 1959). The full range of intervening responses can only be seen in the fast-upstroke model when we use continuation methods rather than numerical integration (Fig. 11E). It is thus not surprising that in the single-channel model one sees both abbreviation and prolongation at $t_c = 117$ ms (Fig. 9B), due to statistical fluctuations in the state of the membrane, which occur prior to delivery of the stimulus pulse, during delivery of the pulse, and after delivery of the pulse. Our simulations with the single-channel model show that for 1000 trials, no intermediate responses are seen (Fig. 10). Fitting Gaussian distributions to the two

peaks in this histogram suggests that an intermediate result in an interval as broad as 25–140 ms will be seen in only one out of every 10,000 trials. However, even if it were possible to carry out an experiment with such a large number of trials, keeping the preparation stationary, and one exceptionally rare intermediate response were found, one could never be certain that, e.g. the electrode had not slightly "unsealed" for that one trial. Thus, in experimental work it is extremely difficult, indeed impossible, to distinguish whether the phase transition curve is truly discontinuous or simply very steep.

Our single-channel model assumes that the individual channels operate independently of each other, i.e. that there is no cooperative behavior in the membrane. However, there is evidence that this is not necessarily the case for several channels, including I_{Na} channels (e.g. Kiss and Nagy, 1985). Cooperative behavior, where opening of one channel promotes the opening of other channels, could be included in differential equations and the single-channel formalism. This would be expected to lead to an enhancement of the abrupt transition.

5.3. Topology of phase-resetting

The transition from type 1 to 0 resetting occurs when the shifted cycle intersects the stable manifold of the fixed point. With the value of −150 pA used in Fig. 11, there is type 1 resetting. At a stimulus amplitude slightly larger than this (−170 pA), type 0 resetting occurs and simulations show that well-timed stimuli can again deliver state points to the vicinity of the slow manifold and the stable manifold of the weak unstable manifold. Whereas in the case of type 1 resetting (Fig. 11E) state points track the weak unstable manifold in the direction of decreasing V until diverging parallel to the strong unstable manifold, in the case of type 0 resetting the exceptional trajectories move along the weak unstable manifold in the direction of increasing V before diverging. Hence, as the stimulus amplitude is varied from −150 to −170 pA, the phase transition curve changes in a continuous manner, with an abrupt transition present in both type 1 and type 0 regions. The presence of an abrupt transition in type 0 resetting has been observed experimentally in aggregates (Vanmeerwijk et al., 1984).

5.4. Applications and significance

Abrupt transitions in the phase transition curve can also occur with hyperpolarizing stimuli delivered to the sinoatrial node (e.g. Jalife et al., 1980) and to the aggregate (Guevara, 1984), and this would also be expected to happen in our model. In terms of autonomic regulation of heart rate, the response of the sinoatrial node to hyperpolarizing stimuli is important, as the parasympathetic input to the sinoatrial node produces hyperpolarization.

Our results are for resetting in a spatially homogeneous system that has traditionally been modelled by nonlinear ordinary differential equations. A related set of considerations apply also to cardiac oscillations that take place in space. For example, it is possible to analyse the resetting of a pacemaker embedded in a sheet of excitable tissue, but stimulated from a distant site within that sheet (Hall and Glass, 1999), or to analyse the resetting of a re-entrant rhythm produced by activity circulating along a one-dimensional ring (Glass and Josephson, 1995) or a two-dimensional annulus (Glass et al., 2002; Sinha et al., 2002; Sinha and Christini, 2002). Questions concerning the continuity of the resetting curves arise in all these circumstances. Since all experimental cardiac systems have some spatial extent, the role of stochastic influences, such as we consider here, in spatially distributed systems is a topic for future study.

The fluctuating opening and closing of the ionic channels in the single-channel implementation introduces noise that is not infinitesimally small. A consequence of this is that a stimulus delivered at a given phase of a cycle may have widely different effects: sometimes it will induce a new action potential but in other cases it will delay an action potential. We believe that stochastic phenomena such as those that are evident here and others (e.g. stochastic fluctuations in vesicular release dynamics in the neuronal control of cardiac rate) do play a role in the genesis of cardiac arrhythmias (Schulte-Frohlinde et al., 2001). A remarkable aspect of clinical electrocardiographic records is that apparently imperceptible differences in cardiac activity can lead to very different outcomes. An abnormal cardiac complex (e.g. a premature ventricular contraction) may in one instance appear as an isolated abnormal beat, while the next instance of an apparently identical premature beat may lead to the onset of a fatal arrhythmia (e.g. ventricular tachycardia or fibrillation). Perhaps it is overly dramatic to imagine that the stochastic opening or closing of a single channel may, in the appropriate context, provide the narrow difference between life and death. Yet, the current work gives at least indirect support to this notion.

Acknowledgements

Art Winfree, through his lectures, his writing, his many conversations with us, and his insightful readings and criticisms of our earlier papers has contributed greatly to our understanding of cardiac rhythms. We dedicate this paper to his memory. We also thank J. Guckenheimer for helpful conversation. TKM thanks the Danish Research Academy and Otto Mønsted's

Foundation for financial support. LG and EJD thank the Natural Sciences and Engineering Research Council and LG and MRG thank the Canadian Institutes for Health Research for support of this work.

Appendix A. Sinoatrial node Hodgkin–Huxley-type models

The rabbit sinoatrial node is an inhomogeneous structure, with the shape of the action potential gradually changing as one moves out from the center of the node towards its periphery. Action potentials recorded in situ from peripheral areas of the sinoatrial node closer to the crista terminalis have a larger maximum upstroke velocity, a higher overshoot potential, a larger maximum diastolic potential, and a shorter action potential duration than those recorded from the central area of the node (Bleeker et al., 1980). These differences are intrinsic, since they persist in small pieces of tissue isolated from mapped locations within the node (Kodama and Boyett, 1985; Kreitner, 1985; Opthof et al., 1987). Also, the interbeat interval is shorter in small pieces isolated from peripheral areas of the node (Kodama and Boyett, 1985; Opthof et al., 1987). Systematic differences in current densities are seen between larger cells and smaller cells in voltage-clamp studies on single cells isolated from the sinoatrial node (Honjo et al., 1996; Lei et al., 2001; Zhang et al., 2000). Since peripherally located cells are larger in situ than central cells, it is generally assumed that larger isolated cells originate from more peripheral areas of the node. The differences in the action potential between smaller and larger isolated sinoatrial node cells parallel the changes seen in multicellular preparations (e.g. the maximal upstroke velocity is higher in larger cells, and the interbeat interval is shorter (Honjo et al., 1996)). Moreover, the current densities in isolated cells change in a manner consistent with the change in their action potential parameters: e.g. the fast inward sodium current (I_{Na}), the delayed rectifier potassium current (I_K), and the hyperpolarization-activated pacemaker current (I_h) are all larger in the larger cells (Honjo et al., 1996; Lei et al., 2001; Zhang et al., 2000), which are presumably of peripheral origin.

We thus develop two models of an isolated sinoatrial node cell, one with the slower upstroke velocity typical of the central sinoatrial node (“slow-upstroke model”), and the other with the faster upstroke velocity typical of the peripheral sinoatrial node (“fast-upstroke model”). Both of these models are modifications of the ionic model of Irisawa and Noma (1982), which is based largely on experiments carried out on strips of rabbit sinoatrial node tissue. The Irisawa–Noma model describes five currents: the fast inward sodium current (I_{Na}), the slow inward current (I_s) carried mainly by Ca^{2+} ions, the delayed rectifier potassium current (I_K), the pacemaker current (I_h), and the time-independent leak current (I_l). We do not use a more complicated “second-generation” model, due to problems with degeneracy and drift (Dokos et al., 1993; Endresen and Skarland, 2000; Guan et al., 1997; Varghese and Sell, 1997). While keeping track of the stimulus current that is injected removes drift in one model, the model remains degenerate (Hund et al., 2001).

A.1. Slow-upstroke model

The upstroke velocity is slow ($\sim 5\,V\,s^{-1}$) in the Irisawa–Noma model. However, I_{Na} recovers from inactivation relatively early on during the action potential. This results in a small secondary peak in the sodium current towards the end of the action potential. This in turn leads to an anomalous bump in the resetting curve when I_{Na} is increased for our fast-upstroke model (developed below). The original formulation of I_{Na} in the Irisawa–Noma model was based on sucrose-gap voltage-clamp experiments on ventricular muscle from various mammalian species (not including the rabbit). We have thus modified the rate constants α_h and β_h (see equations below) so that steady-state inactivation ($h_\infty = \alpha_h/(\alpha_h + \beta_h)$) and the time constant for inactivation ($\tau_h = 1/(\alpha_h/\beta_h)$) are closer to more recent voltage-clamp results on isolated rabbit sinoatrial node cells (Baruscotti et al., 1996; Muramatsu et al., 1996). With these modifications, the time constant for inactivation is much greater and the h_∞-curve is shifted to more hyperpolarized potentials, both of which effects serve to decrease the size of the secondary current peak during the action potential and the anomalous bump in the resetting curves.

As our model of a single cell with a slow upstroke velocity, we use the Irisawa–Noma model with the inactivation process of I_{Na} modified as described immediately above. We set the capacitance to 20 pF (Zhang et al., 2000), which corresponds to the experimental value in the isolated sinoatrial node cells that have slow upstroke velocities and are small in size and presumably of central origin (Honjo et al., 1996; Zhang et al., 2000). We also multiply the maximal conductance of I_{Na} by a factor of 1.3 to retain the same maximal upstroke velocity as in the original Irisawa–Noma model. The maximum diastolic potential also remains unchanged at −66 mV, as does the overshoot potential at 18 mV. The interbeat interval is 338.2 ms and the action potential duration (at 100% repolarization) is 137 ms, which are close to the original Irisawa–Noma values (Guevara and Jongsma, 1990; Irisawa and Noma, 1982).

The equations of the slow-upstroke model are as follows:

$$
\begin{aligned}
dV/dt &= 1/C_m \cdot (I_{Na} + I_K + I_s + I_h + I_l),\\
I_{Na} &= g_{Na} m^3 h (V - 40.0),\\
dm/dt &= \alpha_m (1 - m) - \beta_m m,\\
dh/dt &= \alpha_h (1 - h) - \beta_h h,\\
\alpha_h &= 0.1209 \exp(-(V + 30.0)/6.534),\\
\beta_h &= 10^2/(\exp(-0.1(V + 40.0)) + 0.1),\\
\alpha_m &= 10^3 (V + 37.0)/(1.0 - \exp(-0.1(V + 37.0))),\\
\beta_m &= 4.0 \times 10^4 \exp(-0.056(V + 62.0)),\\
I_K &= g_K p(\exp(0.0277(V + 90.0)) - 1.0)/\\
&\quad \exp(0.0277(V + 40.0)),\\
dp/dt &= \alpha_p (1 - p) - \beta_p p,\\
\alpha_p &= 8.0/(1.0 + \exp(-(V + 4.0)/13.0)),\\
\beta_p &= 0.17(V + 40.0)/\\
&\quad (\exp((V + 40.0)/13.3) - 1.0),\\
I_s &= g_s df(\exp((V - 40.0)/25.0) - 1.0),\\
dd/dt &= \alpha_d (1 - d) - \beta_d d,\\
df/dt &= \alpha_f (1 - f) - \beta_f f,\\
\alpha_d &= 1.2 \times 10^3/(1.0 + \exp(-V/12.0)),\\
\beta_d &= 0.25 \times 10^3/(1.0 + \exp((V + 30.0)/8.0)),\\
\alpha_f &= 0.7(V + 45.0)/(\exp((V + 45.0)/9.5) - 1.0),\\
\beta_f &= 36.0/(1.0 + \exp(-(V + 21.0)/9.5)),\\
I_h &= g_h q(V + 25.0),\\
dq/dt &= \alpha_q (1 - q) - \beta_q q,\\
\alpha_q &= 0.34(V + 100.0)/\\
&\quad (\exp((V + 100.0)/4.4) - 1.0) + 0.0495,\\
\beta_q &= 0.5(V + 40.0)/\\
&\quad (1.0 - \exp(-(V + 40.0)/6.0)) + 0.0845,\\
I_l &= g_l(1.2(1.0 - \exp(-(V + 60.0)/25.0))\\
&\quad + 0.15(V - 2.0)/\\
&\quad (1.0 - \exp(-(V - 2.0)/5.0))),
\end{aligned}
$$

where $C_m = 20\,\text{pF}$, $g_{Na} = 1.3 \times 20 \times 0.5 = 13\,\text{nS}$, $g_K = 20 \times 0.91 = 19.2\,\text{nS}$, $g_s = 20 \times 15 = 300\,\text{nS}$, $g_h = 20 \times 0.2 = 4\,\text{nS}$, and $g_l = 20 \times 1 = 20\,\text{nS}$. Voltage is in mV, time is in s, conductances are in nS, and rate constants are in s^{-1}.

A.2. Fast-upstroke model

In order to obtain a model of a fast-upstroke cell we have modified some of the parameters of the slow-upstroke model in the equations given above. The first change is to increase the capacitance to 65 pF, to reflect the larger capacitance of isolated cells having a fast upstroke velocity (Honjo et al., 1996; Zhang et al., 2000). As in other modelling work on central and peripheral cells (Zhang et al., 2000), we have increased the current densities of the three currents I_{Na}, I_K and I_h in order to obtain a much larger maximal upstroke velocity (71 vs. $5\,\text{V s}^{-1}$), a larger overshoot potential (31 vs. 18 mV), a more hyperpolarized maximum diastolic potential (−78 vs. −66 mV), and a smaller interbeat interval (282 vs. 338 ms) than in the slow-upstroke model. The current density of I_l is unchanged, so that $g_l = 65\,\text{nS}$.

The I_{Na} current density is increased by a factor of 7.7 with respect to the slow-upstroke model so that $g_{Na} = 10 \times 65 \times 0.5 = 325\,\text{nS}$. The peak sodium current density is then in agreement with experiment (Honjo et al., 1996), as is the maximal upstroke velocity of $71\,\text{V s}^{-1}$ (Bleeker et al., 1980; Kodama and Boyett, 1985; Kreitner, 1985; Opthof et al., 1987). As in a previous model (Zhang et al., 2000), we also increase the current density of I_K six-fold, corresponding to the experimental result (Honjo et al., 1996; Lei et al., 2001; Zhang et al., 2000), so that $g_K = 6 \times 65 \times 0.91 = 354.9\,\text{nS}$. This large increase in I_K will tend to hyperpolarize the maximum diastolic potential and abbreviate the action potential duration. We are thus forced to increase the density of I_s two-fold, as was done by Zhang et al. (2000), even though the density of this current is independent of cell size (Honjo et al., 1996), in order to obtain an action potential of sufficiently long duration to compare with that seen in situ (Bleeker et al., 1980), in small pieces (Kodama and Boyett, 1985; Kreitner, 1985; Opthof et al., 1987), and in isolated cells (Honjo et al., 1996). The value of g_s is then $2 \times 65 \times 15 = 1950\,\text{nS}$. The action potential duration in our fast-upstroke model is 86 ms (vs. 137 ms in the slow-upstroke model). As in a previous model (Zhang et al., 2000), we also increase the current density of I_h four-fold, in concordance with the experimental result (Honjo et al., 1996), so that $g_h = 4 \times 65 \times 0.2 = 52\,\text{nS}$. This increase, as well as the increases in the densities of I_{Na} and I_s, will tend to decrease the interbeat interval, which is 282 ms in the fast-upstroke model (vs. 338 ms in the slow-upstroke model).

A.3. Numerical integration

Numerical integration of both models was carried out using a forward Euler routine, i.e. $V(t + \Delta t) = V(t) - \Delta t/C_m \cdot (I_{Na} + I_K + I_s + I_h + I_l + I_{stim})$, where C_m is cell capacitance and I_{stim} is the stimulus current. The integration time step (Δt) was 0.1 ms in most cases for the slow-upstroke model and 0.01 ms in most cases for the fast-upstroke model, but time steps as small as 0.1 μs were used when trying to resolve the abrupt transition in the resetting curve (see Results). Thus, the maximum

changes in voltage were 0.5 mV in the slow-upstroke model and 0.7 mV in the slow-upstroke model. Programs were written in the "C" programming language using "long double" for the precision of real-type variables. The value of any activation or inactivation variable ξ at time $t+\Delta t$ was determined from its value at time t from the analytic formula (Moore and Ramon, 1974) $\xi(t+\Delta t) = \xi_\infty - (\xi_\infty - \xi(t))(e^{-\Delta t/\tau_\xi})$, where ξ_∞ is the steady-state or asymptotic value of ξ ($\xi_\infty = \alpha_\xi/(\alpha_\xi + \beta_\xi)$) and τ_ξ is the time constant of ξ ($\tau_\xi = 1/(\alpha_\xi + \beta_\xi)$) at $V(t)$. Initial conditions for the variables in the slow-upstroke model were $V = -65.8990$ mV, $p = 0.3127$, $d = 0.0197$, $f = 0.5757$, $m = 0.0330$, $h = 0.5168$, and $q = 0.0084$, while in the fast-upstroke model they were $V = -77.5731$ mV, $p = 0.2748$, $d = 0.0083$, $f = 0.5738$, $m = 0.0074$, $h = 0.9990$, and $q = 0.0094$. These initial conditions approximate the point on the limit cycle for each model at the time when V attains the maximum diastolic potential. For the resetting simulations, the model equations were integrated for one full cycle prior to the cycle in which the stimulus was given.

Appendix B. Sinoatrial node single-channel models

B.1. Estimation of single-channel conductances and channel numbers

The first step in converting a Hodgkin–Huxley type of model into a single-channel model is to estimate the single-channel conductance of each current, which is in turn then used to compute the number of single channels responsible for carrying that current. The number of I_K channels per cell (N_K) has been estimated to be 1054 ± 254 in rabbit sinoatrial node cells having an average capacitance of about 35 pF (Shibasaki, 1987). Assuming the same current density in our 20 pF slow-upstroke model, we get $N_K = 600$. For the fast-upstroke model, which has a six-fold higher density in addition to the larger capacitance, we obtain $N_K = 11,000$. In a previous single-channel model (Guevara and Lewis, 1995), the single-channel conductance of I_s was estimated to be 4 pS, which results in the number of I_s channels (N_s) being estimated to be 5250 in a 35 pF model. We scale this to 3000 channels in our slow-upstroke model and 20,000 channels in the fast-upstroke model, which has twice the channel density. In another single-channel model of a rabbit sinoatrial node cell, the single-channel conductance of I_{Na} was estimated to be 20 pS (Wilders and Jongsma, 1993). Using that value, we obtain 650 and 16,300 for the number of I_{Na} channels (N_{Na}) in the slow- and fast-upstroke models respectively. Using the estimated physiological value of 0.5 pS for the single-channel conductance of I_h (Wilders and Jongsma, 1993) gives the number of I_h channels (N_h) to be 8000 and 100,000 in our slow- and fast-upstroke models, respectively.

B.2. Computational method for single-channel model

For the numerical integration of the single-channel models we use a computational method (method 2) described in Skaugen and Walløe (1979). In this method, one keeps track of the ensemble of gates, rather than of each individual gate. That is, one keeps track of the number of channels in each possible state of the ensemble. For the I_K channels, the single gate (p) of the channel is either open or closed. The number of I_K channels in the open and closed states are then NK_0 and NK_1, respectively. The I_s channels have one activation gate (d) and one inactivation gate (f), making the number of I_s channels in the possible states Ns_{00} (both d and f closed), Ns_{01} (d closed, f open), Ns_{10} (d open, f closed), and Ns_{11} (both gates open). The channel is open to pass current only when both gates are open. The pacemaker current I_h passes through a channel with one gate (q). The number of channels with the gate closed is Nh_0, and Nh_1 with the gate open. Finally the I_{Na} channel has one inactivation gate (h) and three activation gates (m). The number of channels in the possible states is NNa_{00} (all gates closed), NNa_{01} (h closed, one m open), NNa_{02} (h closed, two m open), NNa_{03} (h closed, three m open), NNa_{10} (h open, all m closed), NNa_{11} (h open, one m open), NNa_{12} (h open, two m open), NNa_{13} (all gates open). To save computation time, we use an approximation developed by Skaugen and Walløe (1979) (their method 2b), where one does not need to consider all the transitions between the non-open states of the I_{Na} channel (this method has also been previously used in a sinoatrial node single-channel model (Wilders and Jongsma, 1993)). In fact, one need only keep the states NNa_{03} and NNa_{13} stochastic, while setting their neighboring states, NNa_{02} and NNa_{12}, equal to their expected values

$$NNa_{ij} = \binom{3}{j} h^i (1-h)^{1-i} m^j (1-m)^{3-j} N_{Na}, \tag{B.1}$$

where m and h are integrated using the same scheme as in the implementation of the Hodgkin–Huxley-type models (see Appendix A). The lifetime δt of the ensemble in a particular state is given by

$$\begin{aligned}\delta t = &-\ln(r)/\{\alpha_p NK_0 + \beta_p NK_1 + \alpha_q Nh_0 \\ &+ \beta_q Nh_1 + (\alpha_d + \alpha_f) Ns_{00} \\ &+ (\alpha_d + \beta_f) Ns_{01} + (\beta_d + \alpha_f) Ns_{10} \\ &+ (\beta_d + \beta_f) Ns_{11} \\ &+ (\alpha_m + 2\beta_m + \alpha_h) NNa_{02} \\ &+ (3\beta_m + \alpha_h) NNa_{03} \\ &+ (\alpha_m + 2\beta_m + \beta_h) NNa_{12} \\ &+ (3\beta_m + \beta_h) NNa_{13}\},\end{aligned}$$

where r is a pseudorandom number drawn from a uniform distribution on (0,1], α_x is the opening rate

constant of gate x, and β_x is its closing rate constant. After the lifetime of the ensemble (i.e. at $t+\delta t$), a transition will occur to a new state. A second pseudorandom number is drawn. Together with the probability of each particular transition (given as the sum of the probabilities of the different ways in which that transition can occur, divided by the sum of the probabilities of all the possible transitions), this second pseudorandom number determines which new state the system will go to. Finally the voltage is updated using a forward Euler scheme: $V(t+\delta t) = V(t) + \delta V = V(t) - \delta t/C_m\ (I_{\mathrm{Na}} + I_{\mathrm{K}} + I_s + I_h + I_l + I_{stim})$. We did not have to put an upper limit on δt (Skaugen and Walløe, 1979), since in Fig. 3 the maximum value of δt was 0.04 ms in the slow-upstroke model and 0.01 ms in the fast-upstroke model, and the maximum values of δV were 0.01 mV and 0.006 mV, respectively. The leak current is not (pseudo-)randomized, since the ionic nature of this current—in particular, its single-channel conductance—is not known (see Wilders and Jongsma (1993) for exploration of the effect of introducing the single-channel nature of the background current over a range of putative single-channel conductances).

Initial conditions were given by the expected values of the various states at $V = -65.8990$ mV for the slow-upstroke model and at $V = -77.5731$ mV for the fast-upstroke model (same voltages as for the initial conditions in the Hodgkin–Huxley-type models). With all activation and inactivation variables taking on the same initial conditions as in the Hodgkin–Huxley-type model, the expected values for the sodium channel states are given by Eq. (B.1); for the I_{K} channel $NK_i = p^i(1-p)^{1-i}N_{\mathrm{K}}$; for the I_h channel $Nh_i = q^i(1-q)^{1-i}N_h$; and for the I_s channel $Ns_{ij} = d^i(1-d)^{1-i}f^j(1-f)^{1-j}N_s$. As with the Hodgkin–Huxley-type models, the single-channel models were integrated for one full cycle prior to the cycle in which the stimulus pulse was given during a resetting trial. Furthermore, when the time of the start or end of a resetting stimulus pulse fell within the interval $(t, t+\delta t)$, δt was shortened so that a transition of the ensemble occurs exactly at the time when the stimulus is turned on and off (for justification of this, see argument in Skaugen and Walløe, 1979).

Our single-channel model is deterministic, not stochastic, since a deterministic pseudorandom number generator is used to determine lifetimes of the ensemble and the state to which the membrane will switch at the end of each such lifetime. However, ionic channels are presently thought to open and close in a stochastic, not a deterministic fashion (see however Guevara (1991) and Liebovitch and Toth, 1991). Nevertheless, one would be hard pressed to distinguish the output of our pseudorandom single-channel model from that of one in which a truly stochastic random-number generator would be used.

References

Arima, N., Okazaki, H., Nakano, H., 1997. A generation mechanism of canards in a piecewise linear system. IEICE Trans. Fundam. Electron. Commun. Comput. Sci. (Japan) E80-A, 447–453.

Baruscotti, M., DiFrancesco, D., Robinson, R.B., 1996. A TTX-sensitive inward sodium current contributes to spontaneous activity in newborn rabbit sinoatrial node cells. J. Physiol. (London) 492, 21–30.

Bleeker, W.K., Mackaay, A.J.C., Masson-Pévet, M., Bouman, L.N., Becker, A.E., 1980. Functional and morphological organization of the rabbit sinus node. Circ. Res. 46, 11–22.

Chen, P.-S., Wolf, P.D., Dixon, E.G., Daniely, N.D., Frazier, D.W., Smith, W.M., Ideker, R.E., 1988. Mechanism of ventricular vulnerability to single premature stimuli in open-chest dogs. Circ. Res. 62, 1191–1209.

Clay, J.R., 1977. Monte Carlo simulation of membrane noise: an analysis of fluctuations in graded excitation of nerve membrane. J. Theor. Biol. 64, 671–680.

Clay, J.R., DeHaan, R.L., 1979. Fluctuations in interbeat interval in rhythmic heart-cell clusters: role of membrane voltage noise. Biophys. J. 28, 377–389.

Clay, J.R., Guevara, M.R., Shrier, A., 1984. Phase resetting of the rhythmic activity of embryonic heart cell aggregates: experiment and theory. Biophys. J. 45, 699–714.

Clay, J.R., Brochu, R.M., Shrier, A., 1990. Phase resetting of embryonic chick atrial heart cell aggregates: experiment and theory. Biophys. J. 58, 609–621.

Cole, K.S., Guttman, R., Bezanilla, F., 1970. Nerve membrane excitation without threshold. Proc. Natl. Acad. Sci. (USA) 65, 884–891.

Diener, M., 1984. The canard unchained or how slow/fast dynamical systems bifurcate. Math. Intell. 6, 38–49.

Doedel, E.J., Champneys, A.R., Fairgrieve, T.F., Kuznetsov, Y.A., Sandstede, B., Wang, X.-J., 1997. AUTO97: continuation and bifurcation software for ordinary differential equations. Department of Computer Science, Concordia University, Montreal, Canada. http://cmvl.cs.concordia.ca/auto.

Dokos, S., Celler, B.G., Lovell, N.H., 1993. Modification of DiFrancesco–Noble equations to simulate the effects of vagal stimulation on in vivo mammalian sinoatrial node electrical activity. Ann. Biomed. Eng. 21, 321–335.

Endresen, L.P., Skarland, N., 2000. Limit cycle oscillations in pacemaker cells. IEEE Trans. Biomed. Eng. 47, 1134–1137.

FitzHugh, R., 1955. Mathematical models of threshold phenomena in the nerve membrane. Bull. Math. Biophys. 17, 257–278.

FitzHugh, R., 1961. Impulses and physiological states in theoretical models of nerve membrane. Biophys. J. 1, 445–466.

FitzHugh, R., Antosiewicz, H.A., 1959. Automatic computation of nerve excitation—detailed corrections and additions. J. Soc. Ind. Appl. Math. 7, 447–458.

Gedeon, T., Glass, L., 1998. Continuity of resetting curves for FitzHugh–Nagumo equations on the circle. In: Fields Institute Communications, Differential Equations with Applications to Biology, Vol. 21. Springer, New York, pp. 225–236.

Glass, L., Josephson, M.E., 1995. Resetting and annihilation of reentrant abnormally rapid heartbeat. Phys. Rev. Lett. 75, 2059–2062.

Glass, L., Winfree, A.T., 1984. Discontinuities in phase resetting experiments. Am. J. Physiol. 246, R251–R258.

Glass, L., Guevara, M.R., Belair, J., Shrier, A., 1984. Global bifurcations of a periodically forced biological oscillator. Phys. Rev. A 29, 1348–1357.

Glass, L., Nagai, Y., Hall, K., Talajic, M., Nattel, S., 2002. Predicting the entrainment of reentrant cardiac waves using phase resetting curves. Phys. Rev. E 65, 021908.

Guan, S., Lu, Q., Huang, K., 1997. A discussion about the DiFrancesco–Noble model. J. Theor. Biol. 189, 27–32.

Guckenheimer, J., 1975. Isochrons and phaseless sets. J. Math. Biol. 1, 259–273.

Guckenheimer, J., Hoffman, K., Weckesser, W., 2000. Numerical computation of canards. Int. J. Bifurc. Chaos 10, 2669–2687.

Guevara, M.R., 1984. Chaotic cardiac dynamics. Ph.D. Thesis, McGill University, Montreal, Canada.

Guevara, M.R., 1991. Mathematical modeling of the electrical activity of cardiac cells. In: Glass, L., Hunter, P., McCulloch, A. (Eds.), Theory of Heart. Springer, New York, pp. 239–253.

Guevara, M.R., Jongsma, H.J., 1990. Phase resetting in a model of sinoatrial nodal membrane: ionic and topological aspects. Am. J. Physiol. 258, H734–H747.

Guevara, M.R., Lewis, T.J., 1995. A minimal single-channel model for the regularity of beating in the sinoatrial node. Chaos 5, 174–183.

Guevara, M.R., Shrier, A., 1987. Phase resetting in a model of cardiac Purkinje fiber. Biophys. J. 52, 165–175.

Guevara, M.R., Shrier, A., Glass, L., 1986. Phase resetting of spontaneously beating embryonic ventricular heart cell aggregates. Am. J. Physiol. 251, H1298–H1305.

Hall, K., Glass, L., 1999. How to tell a target from a spiral: the two probe problem. Phys. Rev. Lett. 82, 5164–5167.

Honjo, H., Boyett, M.R., Kodama, I., Toyama, J., 1996. Correlation between electrical activity and the size of rabbit sino-atrial node cells. J. Physiol. (London) 496, 795–808.

Hund, T.J., Kucera, J.P., Otani, N.F., Rudy, Y., 2001. Ionic charge conservation and long-term steady state in the Luo–Rudy dynamic cell model. Biophys. J. 81, 3324–3331.

Irisawa, H., Noma, A., 1982. Pacemaker mechanisms of rabbit sinoatrial node cells. In: Bouman, L.N., Jongsma, H.J. (Eds.), Cardiac Rate and Rhythm. Nijhoff, The Hague, pp. 35–51.

Jalife, J., Antzelevitch, C., 1979. Phase resetting and annihilation of pacemaker activity in cardiac tissue. Science 206, 695–697.

Jalife, J., Moe, G.K., 1976. Effect of electrotonic potentials on pacemaker activity of canine Purkinje fibers in relation to parasystole. Circ. Res. 39, 801–808.

Jalife, J., Hamilton, A.J., Lamanna, V.R., Moe, G.K., 1980. Effects of current flow on pacemaker activity of the isolated kitten sionatrial node. Am. J. Physiol. 238, H307–H316.

Kawato, M., 1981. Transient and steady state phase response curves of limit cycle oscillators. J. Math. Biol. 12, 13–30.

Kawato, M., Suzuki, R., 1978. Biological oscillators can be stopped—topological study of a phase response curve. Biol. Cybern. 30, 241–248.

Kiss, T., Nagy, K., 1985. Interaction between sodium channels in mouse neuroblastoma cells. Eur. Biophys. J. 12, 13–18.

Kodama, I., Boyett, M.R., 1985. Regional differences in the electrical activity of the rabbit sinus node. Pflügers Arch. 404, 214–226.

Kreitner, D., 1985. Electrophysiological study of the two main pacemaker mechanisms in the rabbit sinus node. Cardiovasc. Res. 19, 304–318.

Lei, M., Honjo, H., Kodama, I., Boyett, M.R., 2001. Heterogeneous expression of the delayed-rectifier K^+ currents $i_{K,s}$ and $i_{K,r}$ in rabbit sinoatrial node cells. J. Physiol. (London) 535, 703–714.

Liebovitch, L.S., Toth, T.I., 1991. A model of ion channel kinetics using deterministic chaotic rather than stochastic processes. J. Theor. Biol. 148, 243–267.

Moore, J.W., Ramon, F., 1974. On numerical integration of the Hodgkin and Huxley equations for a membrane action potential. J. Theor. Biol. 45, 249–273.

Muramatsu, H., Zou, A.-R., Berkowitz, G.A., Nathan, R.D., 1996. Characterization of a TTX-sensitive Na^+ current in pacemaker cells isolated from rabbit sinoatrial node. Am. J. Physiol. 270, H2108–H2119.

Opthof, T., van Ginneken, A.C.G., Bouman, L.N., Jongsma, H.J., 1987. The intrinsic cycle length in small pieces isolated from the rabbit sinoatrial node. J. Mol. Cell. Cardiol. 19, 923–934.

Schulte-Frohlinde, V., Ashkenazy, Y., Ivanov, P.Ch., Glass, L., Goldberger, A.L., Stanley, H.E., 2001. Noise effects on the complex patterns of abnormal heartbeats. Phys. Rev. Lett. 87, 068104.

Shibasaki, T., 1987. Conductance and kinetics of delayed rectifier potassium channels in nodal cells of the rabbit heart. J. Physiol. (London) 387, 227–250.

Sinha, S., Christini, D.J., 2002. Termination of reentry in an inhomogeneous ring of model cardiac cells. Phys. Rev. E 66, 061903.

Sinha, S., Stein, K.M., Christini, D.J., 2002. Critical role of inhomogeneities in pacing termination of cardiac reentry. Chaos 12, 893–902.

Skaugen, E., Walløe, L., 1979. Firing behaviour in a stochastic nerve membrane model based upon the Hodgkin–Huxley equations. Acta Physiol. Scand. 107, 343–363.

Vanmeerwijk, W.P.M., Debruin, G., van Ginneken, A.C.G., Vanhartevelt, J., Jongsma, H.J., Kruyt, E.W., Scott, S.S., Ypey, D.L., 1984. Phase resetting properties of cardiac pacemaker cells. J. Gen. Physiol. 83, 613–629.

Varghese, A., Sell, G.R., 1997. A conservation principle and its effect on the formulation of Na–Ca exchanger current in cardiac cells. J. Theor. Biol. 189, 33–40.

Wiggins, S., 1988. Global Bifurcations and Chaos. Springer, New York.

Wilders, R., 1993. From single channel kinetics to regular beating. Ph.D. thesis, University of Amsterdam, Amsterdam, The Netherlands.

Wilders, R., Jongsma, H.J., 1993. Beating irregularity of single pacemaker cells isolated from the rabbit sinoatrial node. Biophys. J. 65, 2601–2613.

Winfree, A.T., 1970. The temporal morphology of a biological clock. In: Gerstenhaber, M. (Ed.), Lectures on Mathematics in the Life Sciences, Vol. 2. American Mathematical Society, Providence, RI, pp. 109–150.

Winfree, A.T., 1980. The Geometry of Biological Time, 1st Edition. Springer, New York.

Winfree, A.T., 2000. The Geometry of Biological Time, 2nd Edition. Springer, New York.

Zhang, H., Holden, A.V., Kodama, I., Honjo, H., Lei, M., Varghese, T., Boyett, M.R., 2000. Mathematical models of action potentials in the periphery and center of the rabbit sinoatrial node. Am. J. Physiol. 279, H397–H421.